BJ Biomolecules

Biochem. J. (2014) **461**, 413–426 (Printed in Great Britain) doi:10.1042/BJ20140219

online data

Aβ dimers differ from monomers in structural propensity, aggregation paths and population of synaptotoxic assemblies

Tiernan T. O'MALLEY*†, Nur Alia OKTAVIANI‡, Dainan ZHANG§, Aleksey LOMAKIN‖, Brian O'NUALLAIN*, Sara LINSE¶, George B. BENEDEK‖, Michael J. ROWAN§, Frans A. A. MULDER‡**[1] and Dominic M. WALSH*[1]

*Laboratory for Neurodegenerative Research, Center for Neurologic Diseases, Brigham and Women's Hospital, and Harvard Medical School, Boston, MA 02115, U.S.A.
†School of Biomolecular and Biomedical Science, University College Dublin, Dublin 4, Republic of Ireland
‡Groningen Biomolecular Sciences and Biotechnology Institute, University of Groningen, 9749 AB Groningen, The Netherlands
§Department of Pharmacology and Therapeutics, Trinity College, Dublin 2, Ireland
‖Department of Physics and Materials Processing Center, Massachusetts Institute of Technology, Cambridge, MA 02139, U.S.A.
¶Department of Biophysical Chemistry, Lund University, SE221 00 Lund, Sweden
**Interdisciplinary Nanoscience Center (iNANO), Department of Chemistry, Aarhus University, DK-8000 Aarhus C, Denmark

Dimers of Aβ (amyloid β-protein) are believed to play an important role in Alzheimer's disease. In the absence of sufficient brain-derived dimers, we studied one of the only possible dimers that could be produced *in vivo*, $[A\beta]_{DiY}$ (dityrosine cross-linked Aβ). For comparison, we used the Aβ monomer and a design dimer cross-linked by replacement of Ser^{26} with cystine $[A\beta S26C]_2$. We showed that similar to monomers, unaggregated dimers lack appreciable structure and fail to alter long-term potentiation. Importantly, dimers exhibit subtly different structural propensities from monomers and each other, and can self-associate to form larger assemblies. Although $[A\beta]_{DiY}$ and $[A\beta S26C]_2$ have distinct aggregation pathways, they both populate bioactive soluble assemblies for longer durations than Aβ monomers. Our results indicate that the link between Aβ dimers and Alzheimer's disease results from the ability of dimers to further assemble and form synaptotoxic assemblies that persist for long periods of time.

Key words: Alzheimer's disease, amyloid β-protein, long-term potentiation, nuclear magnetic resonance (NMR), synaptic plasticity.

INTRODUCTION

AD (Alzheimer's disease) represents a personal and societal tragedy of enormous proportions [1]. Strong genetic evidence links the APP (amyloid precursor protein) and its proteolytic derivatives to AD [2]. A leading hypothesis proposes that a small amphipathic fragment of APP, the Aβ (amyloid β-protein), self-associates to form assemblies loosely referred to as oligomers, and that these trigger a complex pathogenic sequence of events that culminate in dementia [3–6]. Several mutations within the Aβ sequence cause early-onset AD and are believed to increase the formation of toxic Aβ assemblies (reviewed in [7]). However, such mutations are very rare and most cases of AD occur in individuals with the normal Aβ sequence. Why wild-type Aβ folds to form toxic assemblies is unclear and may involve both intrinsic and extrinsic factors. One possibility is that certain post-translational modifications of Aβ may arise in some individuals and that these lead to sufficiently high levels of toxic Aβ assemblies so as to precipitate sporadic AD.

Although the forms of Aβ that mediate memory impairment and the toxic pathways activated by Aβ remain unresolved, numerous studies have shown that non-fibrillar water-soluble Aβ from a variety of sources are potent synaptotoxins [8–10]. Post-mortem studies indicate that elevated levels of water-soluble Aβ are specific for AD [11–14] and *in vitro* studies show that such material robustly inhibits LTP (long-term potentiation), facilitates LTD (long-term depression) and induces tau hyperphosphorylation and neuritic degeneration [10,15,16]. Aβ from bioactive AD brain extracts migrates on SDS/PAGE (16 % gel) as broad bands centred at ~4 and ~8 kDa. In an earlier study, we fractionated aqueous extract from an AD brain using SEC (size-exclusion chromatography) and Aβ eluted in fractions consistent with monomer, dimer and high-molecular-mass species of undefined size [10]. Testing of each fraction revealed that the dimer fraction, but not the monomer fraction, blocked LTP [10]. However, since fractions were frozen, freeze-dried and reconstituted in artificial cerebrospinal fluid, and then used in LTP experiments [10], it is unclear whether the activity attributed to dimers was mediated by dimers, or assemblies formed by dimers. Indeed, we have demonstrated that the plasticity-disrupting activity originally attributed to a covalent dimer [10] was in fact mediated by soluble aggregates formed from this dimer [17]. Owing to the technical difficulties in studying freshly size-isolated brain dimers, it remains unclear whether native dimers have direct synaptotoxic activity or whether they gain activity by forming larger structures.

Abbreviations: Aβ, amyloid β-protein; $[A\beta]_{DiY}$, dityrosine cross-linked Aβ; $[A\beta S26C]_2$, design Aβ dimer cross-linked by replacement of Ser^{26} with cystine; AD, Alzheimer's disease; APP, amyloid precursor protein; DiY, dityrosine; DSS, 2,2-dimethyl-2-silapentane-5-sulfonic acid; EPSP, excitatory postsynaptic potential; HFS, high-frequency stimulation; LTP, long-term potentiation; ncSPC, neighbour-corrected structural propensity calculator; QLS, quasi-elastic light scattering; RFU, relative fluorescent unit; R_H, hydrodynamic radius; SEC, size-exclusion chromatography; $t_{1/2max}$, 50 % of maximal ThT binding; ThT, thioflavin T.

[1] Correspondence may be addressed to either of these authors (email fmulder@chem.au.dk or dwalsh3@partners.org).

How brain dimers form and interactions that govern the association of component monomers remains enigmatic. In the absence of sufficient highly pure brain-derived Aβ dimers, we and others have used synthetic dimers to gain insight into the natural species. In earlier studies, Aβ(1–40) containing a cysteine residue in place of Ser^{26} was used to produce disulfide cross-linked dimers [Aβ(1–40)S26C]$_2$. Such dimers rapidly aggregated to form protofibrils, and similar to brain-derived Aβ, potently inhibited LTP [10,17], facilitated aberrant phosphorylation of tau and induced neuritic degeneration [16]. Aβ dimers produced by introduction of the cystine residue at either the N- or C-terminus of Aβ [e.g. Aβ(1–40)A2C and Aβ(1–40)-GGGC] also rapidly aggregated to form kinetically trapped protofibrils [18]. Similarly, dimers formed by alkyl cross-linking of alanine residues introduced at position 10 aggregated without a detectable time lag [19]. Although, in Nature, mutations that introduce cysteine residues into the Aβ sequence or promote alkylizing cross-links have not been found, certain post-translational modifications have the potential to covalently link two (or more) Aβ monomers. One possibility would involve the phenolic coupling of tyrosine residues. DiY (dityrosine) cross-linking can result from an increase in oxidative stress and a number of different tyrosine-containing proteins are known to form DiY [20]. Importantly, DiY cross-linking is increased in the AD brain [21] and a recent immuno-EM report detected DiY in amyloid plaques that co-stained for Aβ [22]. Moreover, in test tube experiments, Aβ can be readily induced to form [Aβ]$_{DiY}$ (dityrosine cross-linked Aβ) [22–25].

In the present study, we sought to investigate the structures of wild-type Aβ monomer, [Aβ]$_{DiY}$ and [AβS26C]$_2$ (design Aβ dimer cross-linked by replacement of Ser^{26} with cystine), and to relate these structures to measures of aggregation and toxicity. Since chemically synthesized peptides have certain limitations [26], we were careful to study both synthetic and recombinant versions of each peptide. These included the synthetic peptides Aβ(1–40), [Aβ(1–40)S26C]$_2$, [Aβ(1–40)]$_{DiY}$ and the corresponding recombinant peptides which contain an exogenous N-terminal methonine residue and are designated as Aβ(M1–40), [Aβ(M1–40)S26C]$_2$ and [Aβ(M1–40)]$_{DiY}$ (Supplementary Figure S1 at http://www.biochemj.org/bj/461/bj4610413add.htm). Recombinant expression is particularly well suited for the generation of isotopically labelled Aβ peptides necessary for NMR experiments. 2D (^{13}C,^{1}H)-HSQC NMR spectra are highly similar for Aβ(M1–40), [Aβ(M1–40)S26C]$_2$, [Aβ(M1–40)]$_{DiY}$ with ^{13}Cα,^{1}Hα cross-peak differences between the dimers and wild-type monomer mainly located around the sites of covalent cross-linking. However, using chemical shift differences to estimate the propensity for secondary structure, we found that [Aβ(M1–40)S26C]$_2$ has a slightly greater propensity to form β-sheet structure than wild-type monomer. On the other hand, [Aβ(M1–40)]$_{DiY}$ displays a slight increase in helicity throughout the Aβ molecule, except at the extreme C-terminus. In addition, the aggregation propensity and products formed by the three peptides are very different.

Aggregation of monomer is characterized by a short, but discernible, lag phase after which aggregates are formed more rapidly, producing bundles of laterally associated amyloid fibrils, whereas [AβS26C]$_2$ aggregates without a time lag and forms protofibrils. The behaviour of [Aβ]$_{DiY}$ is distinct from both the other two peptides, with [Aβ]$_{DiY}$ aggregating very slowly to form long smooth individual amyloid fibrils. Despite the fact that these peptides aggregate at very different rates to form different end-products, all three can form neuroplasticity-disrupting assemblies. Thus it appears that the synaptotoxic activity of aggregate intermediates is not readily related to the starting structure of Aβ monomers or dimers, or to the end-stage aggregates they form, but better relates to the size of intermediates. The finding that dimers populated aggregation intermediates for prolonged periods (relative to those formed by monomer) suggests that dimers may be the cause of the synaptic dysfunction that characterizes AD.

MATERIALS AND METHODS

Reagents

Unless otherwise stated, all chemicals and reagents were purchased from Sigma–Aldrich and were of the highest purity available. Synthetic peptides, Aβ(1–40) and Aβ(1–40)S26C, were synthesized and purified using reverse-phase HPLC by Dr James I. Elliott at Yale University (New Haven, CT, U.S.A.). Peptide mass and purity (>99 %) were confirmed by electrospray/ion trap MS, reverse-phase HPLC and SDS/PAGE with silver staining.

Bacterial expression of Aβ peptides

Recombinant Aβ(M1–40) and Aβ(M1–40)S26C were expressed and purified essentially as described previously [27]. pET vectors containing a synthetic gene beginning with AUG (start codon, methionine) followed by the sequence for both Aβ(1–40) wild-type and Ser^{26} substituted for cysteine residue, Aβ(1–40)S26C, were used to transform *Escherichia coli* BL21* DE3 pLysS cells (Promega Biosciences). Cells with the appropriate vector were grown on LB agar plates containing 50 μg/ml ampicillin and 38 μg/ml chloramphenicol. A single colony was transferred to 50 ml of LB medium (containing antibiotics) and incubated for 12 h at 37 °C in an orbital shaker-incubator at 120 rev./min. The starter culture was used to inoculate (at 100-fold dilution) 400 ml aliquots of LB medium and incubated at 37 °C with shaking at 120 rev./min. Cell density was measured every 45 min and when attenuance at 600 nm reached ~0.6, peptide expression was induced by the addition of IPTG. Bacterial cells were collected by centrifugation and pelleted from a 400 ml culture snap-frozen in 25 ml of 10 mM Tris/HCl, pH 8.5, containing 1 mM EDTA (buffer A). Pellets were thawed at room temperature and sonicated. The sonicated suspension was collected by centrifugation at 18 000 ***g*** and the supernatant discarded. The pellet was resuspended in 25 ml of buffer A, sonicated and centrifuged as above. Following three rounds of sonication in buffer A, inclusion bodies containing Aβ were solubilized in 15 ml of 8 M urea/buffer A with sonication and cleared of insoluble debris by centrifugation.

Purification of recombinant Aβ peptides

The inclusion bodies solution was diluted in a ratio of 1:4 with buffer A and incubated at room temperature with Whatman DE23 anion-exchange resin and gently agitated for 30 min. The DE23 resin was isolated using a vacuum filter and washed with buffer A containing 25 mM NaCl. Aβ was eluted in buffer A containing 125 mM NaCl. Aβ-containing fractions were pooled, transferred to a 3 kDa MWCO (molecular-mass cut-off) dialysis sac (Thermo Scientific) and extensively dialysed against 10 mM ammonium bicarbonate, pH 8.5, and the dialysate freeze-dried. Semi-purified bacterial extract (25 mg) was dissolved in 3 ml of 7 M guanidine hydrochloride in 50 mM Tris/HCl, pH 8.5, containing 5 mM EDTA in the presence or absence of 2.5 % 2-mercaptoethanol and Aβ further purified on a Superdex 75 16/60 column (GE Healthcare) eluted in 50 mM ammonium bicarbonate, pH 8.5, at 0.8 ml/min. Peak fractions were pooled

and the peptide concentration was determined by molar absorption coefficient ε_{275} (1361 $M^{-1} \cdot cm^{-1}$) (Supplementary Figure S2 at http://www.biochemj.org/bj/461/bj4610413add.htm). Aliquots of peptide ranging from 0.5 to 5 mg were freeze-dried. All peptides were at least 99.9 % pure as determined by SDS/PAGE or silver staining and reverse-phase HPLC. Peptide mass was confirmed by MALDI–TOF-MS.

Oxidative cross-linking of Aβ peptides

Aliquots (5 mg) of Aβ(1–40) or Aβ(M1–40) were dissolved in 0.5 ml of 7 M guanidine hydrochloride and purified on a Superdex 75 10/300 column (GE Healthcare), and then eluted in 50 mM ammonium bicarbonate, pH 8.5. Peak fractions were collected and pooled, and peptide concentration determined by molar absorption coefficient ε_{275}. The sample was then diluted to 40 μM and incubated at 37 °C overnight in the presence of 2.2 μM horseradish peroxidase (Thermo Scientific) and 250 μM H_2O_2 [28]. Reduced AβS26C monomer was diluted to 40 μM and incubated at room temperature and bubbled with oxygen for 5 min every 24 h for 72 h [17]. Following cross-linking, the reaction mixtures were freeze-dried. Freeze-dried peptides were redissolved in 3 ml of 7 M guanidine hydrochloride and incubated overnight at room temperature and the Aβ dimer was isolated using a Superdex 75 16/60 column eluted in 50 mM ammonium bicarbonate. Peak fractions of dimer were pooled and their concentration determined by A_{275} for $[A\beta S26C]_2$ ($\varepsilon = 2722\ M^{-1} \cdot cm^{-1}$) and A_{283} for $[A\beta]_{DiY}$ ($\varepsilon = 6226\ M^{-1} \cdot cm^{-1}$, Supplementary Figure S2).

ThT (thioflavin T) dye-binding assay

The peptide was dissolved in 7 M guanidine hydrochloride and incubated overnight at room temperature and used for SEC as described above. Aggregation was monitored using a continuous ThT-binding assay. Samples were diluted with a 100-fold ThT stock to 20 μM ThT and the highest stock concentration of Aβ peptide (40 μM–20 μM) and where appropriate this was diluted using SEC elution buffer containing ThT. Six 120 μl replicates of each Aβ concentration were transferred to a black flat bottom, 96-well polystyrene plate (Fisher Scientific). A blank (no peptide containing) sample was also prepared. The outer edge wells of the plate were filled with buffer. At zero time ($t = 0$), plates were analysed on a SpectraMax M2 microplate reader (Molecular Devices) with 5 s of shaking before readings ($\lambda_{em} = 435$ nm and $\lambda_{em} = 485$ nm). Plates were sealed with an adhesive cover and incubated at 37 °C with or without shaking at 700 rev./min in a WorTemp 56 incubator/shaker (3 mm orbit; Labnet International). Plates were removed from the incubator-shaker at regular intervals and the fluorescence was measured. Lag time is defined as the first of two consecutive time points showing a statistically significant increase (Student's t test) in fluorescence compared with the $t = 0$ reading; the rate of aggregation is given by the maximum slope of the linear phase of aggregation [29].

In order to produce the $t_{½max}$ and t_{max} material used for LTP experiments, a preliminary experiment was conducted using 20 μM of each peptide as described above. The maximal fluorescence and the time taken to attain half maximal fluorescence were used to guide the subsequent experiment in which $t_{½max}$ or t_{max} samples were prepared. In the second phase of the experiment, peptide samples were isolated and prepared exactly as in the preliminary experiment, but this time, two replicates were incubated with ThT and four replicates without. Fluorescence was monitored for the samples containing ThT. When readings equal to the $t_{½max}$ or t_{max} values obtained in the preliminary experiment were reached, the samples without ThT were then collected, separated into aliquots and frozen. Monitoring of the samples containing ThT was continued until maximal aggregation was achieved.

Negative stain EM

Samples (10 μl) were applied to carbon-coated Formvar grids for 1 min and then cross-linked using 10 μl of 0.5 % gluteraldehyde. Grids were washed gently with Milli-Q water (Millipore), stained for 2 min with 2 % uranyl acetate (Electron Microscope Sciences) and blotted dry. Samples were prepared in duplicate and examined using a Tecnai G^2 Spirit BioTWIN electron microscope (FEI). EM grids were scanned in a serpentine fashion at ∼×12000, then regions of interest were examined at higher magnification and images captured with an AMT 2k CCD (charge-coupled-device) camera.

Animals and surgery

Experiments were carried out on urethane (1.5–1.6 g/kg of body mass via intraperitoneal injection)-anaesthetized male Wistar rats (250–300 g). The body temperature of the rats was maintained at 37–38 °C with a feedback-controlled heating blanket. The animal care and experimental protocol were approved by the Department of Health, Republic of Ireland.

Cannula and electrode implantation

A stainless-steel cannula (22 gauge, 0.7 mm outer diameter) was implanted above the right lateral ventricle (1 mm lateral to the midline, 0.5 mm posterior to the bregma and 4 mm below the surface of the dura). Intracerebroventricular injection was made via an internal cannula (28 gauge, 0.36 mm outer diameter). The solutions were injected at ∼1 μl per min (total volume 8 μl). Verification of the placement of cannula was performed post mortem by checking the spread of ink dye after intracerebroventricular injection. The dose of Aβ chosen for injection was based on initial pilot dose titration experiments and our previous results [30]. Twisted bipolar electrodes were constructed from Teflon-coated tungsten wires (62.5 μm inner core diameter, 75 μm external diameter). Field EPSPs (excitatory postsynaptic potentials) were recorded from the stratum radiatum in the CA1 area of the right hippocampus in response to stimulation of the ipsilateral Schaffer collateral–commissural pathway. Electrode implantation sites were identified using stereotaxic co-ordinates relative to the bregma, with the recording site located 3.4 mm posterior to bregma and 2.5 mm lateral to midline, and stimulating site 4.2 mm posterior to bregma and 3.8 mm lateral to midline. The final placement of electrodes was optimized by using electrophysiological criteria and confirmed via post-mortem analysis.

Electrophysiology and data analysis

Test EPSPs were evoked by square wave pulses (0.2 ms duration) at a frequency of 0.033 Hz and an intensity that triggered a 50 % maximum response. LTP was induced using 200 Hz HFS (high-frequency stimulation) consisting of three sets of ten trains of 20 stimuli (inter-set intervals, 5 min). The stimulation intensity was not changed during HFS. The magnitude of LTP is expressed as the percentage of pre-HFS baseline EPSP amplitude

(mean ± S.E.M.). One-way ANOVA was used to compare the magnitude of LTP for the last 10 min (i.e. at 3 h) post-HFS between multiple groups. Student's t test and Bonferroni's test were used for detailed statistical analysis where appropriate and $P < 0.05$ was considered statistically significant.

Analytical SEC

Samples (10 μl) were loaded on to a Superdex 75 3.2/300 PE column, eluted at 0.05 ml/min and the A_{214} was recorded. For $t_{1/2max}$ and t_{max}, samples were first centrifuged at 16000 ***g*** for 30 min to remove any insoluble aggregates.

QLS (quasi-elastic light scattering)

Samples were collected directly from a Superdex 75 10/300 column into a borosilicate glass test tube [31] and immediately analysed by QLS. Thereafter, samples were incubated at 4 °C for 2 h, then re-analysed by QLS and the analysis continued for a further 22 h. Measurements were made using a custom optical setup [32] comprising a 40 mW He-Ne laser ($\lambda = 633$ nm) (Coherent) and a PD4047 detector/correlator unit (Precision Detectors). Light scattering was measured at 90°. The intensity correlation function and the distribution of the R_H (hydrodynamic radii) of the particles contributing to the scattering were determined using Precision Deconvolve software (Precision Detectors).

CD

Samples at given time points were diluted to 100 μM monomer or 50 μM dimer and transferred to a 1 mm quartz cuvette (Starna Scientific). Spectra were recorded at 4 °C between 280 nm and 190 nm with 0.2 nm intervals and 20 nm/min continuous scanning using a J-185 CD spectropolarimeter (JASCO). Curves generated from the average of three accumulations were manipulated by subtracting the blank buffer signal and smoothened using a means-movement function with a convolution width of 15 data points. Data are shown as mean molar ellipticity (θ).

NMR spectroscopy

To obtain isotopically labelled Aβ(M1–40) and Aβ(M1–40)S26C, transformed bacteria were grown in M9 minimal medium containing 4 g/l D-[^{13}C]glucose and 1 g/l $^{15}NH_4Cl$ (Cambridge Isotope) [33] and purified as described above (Supplementary Figure S3 at http://www.biochemj.org/bj/461/bj4610413add.htm). [U-^{13}C,^{15}N]Aβ(M1–40) (2 mg), 3 mg of [U-^{13}C,^{15}N][Aβ(M1–40)]$_{DiY}$ or 3 mg of [U-^{13}C,^{15}N][Aβ(M1–40)S26C]$_2$ were dissolved in 0.5 ml of 7 M guanidine hydrochloride and incubated overnight at room temperature. Aβ monomers or dimers were isolated by SEC as described above, but eluted in 25 mM ammonium bicarbonate, pH 8.0. Peak fractions were collected and peptide concentration determined at A_{275} or A_{283}. Samples were diluted to ~200 μM in an NMR tube containing 0.15 mM DSS (2,2-dimethyl-2-silapentane-5-sulfonic acid) and 10 % ^2H_2O. All experiments were carried out on a Varian Unity INOVA 600 MHz spectrometer equipped with a pulsed field gradient probe at 278 K. Backbone $^1H\alpha$, $^{13}C\alpha$ and $^{13}C'$ chemical shifts were assigned based on 2D-NMR experiments, such as (^{13}C,^{1}H)-HSQC (aliphatic region), CO(CA)H, HA(CA)N, (^{15}N,^{1}H)-HSQC, as well as 3D HNCO and HNCA. All spectra were processed using NMRPipe [34] and analysed using Sparky [35] (http://www.cgl.ucsf.edu/home/sparky/). Chemical shifts were referenced to DSS based on IUPAC recommendation [36]. Structural propensities of Aβ(M1–40), [Aβ(M1–40)]$_{DiY}$ and [Aβ(M1–40)S26C]$_2$ were calculated using ncSPC (neighbour-corrected structural propensity calculator) [37,38].

RESULTS

[Aβ(1–40)]$_{DiY}$ and [Aβ(1–40)S26C]$_2$ exhibit very different aggregation kinetics from one another and from Aβ(1–40) monomer

In agreement with our previous study, [Aβ(1–40)S26C]$_2$ readily aggregated under quiescent conditions to form kinetically trapped protofibril-like species [17], whereas even after 96 h, neither Aβ(1–40) or [Aβ(1–40)]$_{DiY}$ formed detectable aggregates (Figure 1A). However, when samples were agitated, both Aβ(1–40) and [Aβ(1–40)]$_{DiY}$ did aggregate. Aβ(1–40) produced ThT-positive species after a time lag of 40–60 min and the maximal rate and extent of aggregation was directly dependent on concentration (Figure 1C). In five out of six separate experiments, the lag for the highest concentration (20 μM) was always the shortest, and the lag for the lowest concentration (2.5 μM) the longest, but due to the 20 min sampling intervals, it was often difficult to differentiate lag times for the intermediate concentrations. Aggregates present at the end of the time course appear as meshes of laterally associated fibrils of approximately 11 ± 2 nm in width (Figure 1, and Supplementary Figure S4 at http://www.biochemj.org/bj/461/bj4610413add.htm). In contrast, [Aβ(1–40)]$_{DiY}$ exhibits a prolonged lag phase compared with Aβ(1–40) and only shows significant ThT binding at concentrations ⩾20 μM and after ⩾10 h of incubation (Figure 1, and Supplementary Figure S5 at http://www.biochemj.org/bj/461/bj4610413add.htm). The apparent aggregation rate of 20 μM [Aβ(1–40)]$_{DiY}$ is ~15-fold lower than the rate observed for 20 μM Aβ(1–40) (Figure 1), and the structures formed are very different. [Aβ(1–40)]$_{DiY}$ produces individual fibrils several microns long, with a periodicity of ~187 ± 29 nm and width of ~10 ± 2 nm (Figure 1 and Supplementary Figure S4). The dramatically lower rate of aggregation for [Aβ(1–40)]$_{DiY}$ is in accordance with a recent report on the aggregation kinetics of this peptide [39]. As with quiescent conditions, when agitated [Aβ(1–40)S26C]$_2$ aggregated without a lag (Figure 1 and Supplementary Figure S5). At 20 μM [Aβ(1–40)S26C]$_2$, ThT fluorescence increases continuously from 0 h to 4 h [rate ~1.0 RFU (relative fluorescent units)/min] (Supplementary Figure S5) and plateaus after approximately 30 h (Figure 1). EM revealed that even after prolonged incubation, [Aβ(1–40)S26C]$_2$ assembles to form short structures only (length, 85 ± 40 nm; width, 10 ± 2 nm) (Figure 1 and Supplementary Figure S4), but, in general, these appear more straight and rigid than protofibrils formed under quiescent conditions (Figure 1B). Given the dramatic difference in the aggregation propensities and ultrastructures of aggregates formed by the three different peptides, we were anxious to investigate the disease-relevant activity of aggregates formed by each peptide.

Aggregated Aβ(1–40), [Aβ(1–40)]$_{DiY}$ and [Aβ(1–40)S26C]$_2$, but not their monomer/dimer precursors, inhibit LTP in the live rat

Changes in the metabolism of Aβ occur 15–20 years in advance of overt symptoms of AD [40,41] and long before detectable neuronal loss, and Aβ is postulated to chronically disrupt synaptic efficacy and episodic memory [42]. LTP is a cellular correlate of

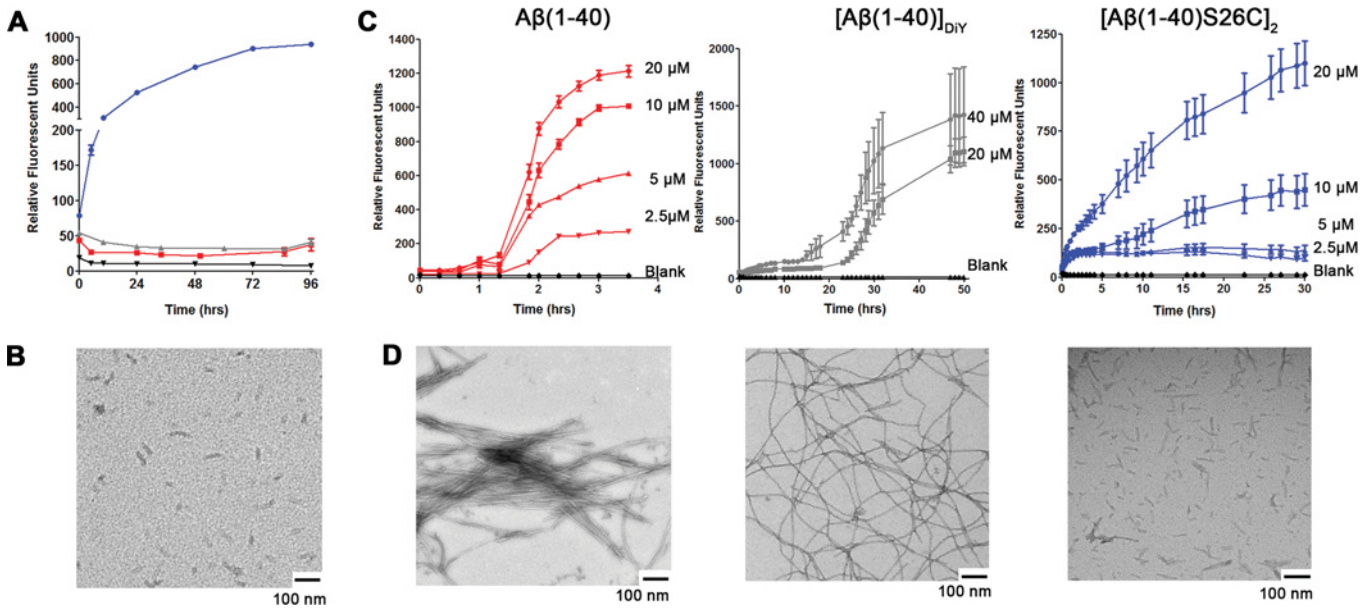

Figure 1 Aβ(1–40), [Aβ(1–40)]$_{DiY}$ and [Aβ(1–40)S26C]$_2$ aggregate at different rates and form different products

(**A**) SEC-isolated Aβ(1–40) (red squares), [Aβ(1–40)]$_{DiY}$ (grey triangles) and [Aβ(1–40)S26C]$_2$ (blue circles) were diluted to 20 μM with 20 mM sodium phosphate, pH 7.4, combined with 20 μM ThT and incubated at 37 °C. As a control, buffer alone (black triangles) was also analysed. Fluorescence was measured at regular intervals. Each point is the means ± S.E.M. for six replicates. (**B**) The end point [Aβ(1–40)S26C]$_2$ was examined by negative stain EM. (**C**) SEC-isolated Aβ(1–40) (red), [Aβ(1–40)]$_{DiY}$ (grey) or [Aβ(1–40)S26C]$_2$ (blue) (2.5–40 μM) in 20 mM sodium phosphate, pH 8.0, were combined with 20 μM ThT. Samples were incubated at 37 °C with shaking and ThT fluorescence monitored at regular intervals. Each point is the means ± S.E.M. for six replicates. The curves were generated by joining data symbols point to point. (**D**) Representative EM images from end point samples (for additional images, see Supplementary Figure S4 at http://www.biochemj.org/bj/461/bj4610413add.htm). The results shown are representative of at least three experiments.

learning and memory that is exquisitely sensitive to disruption by Aβ [43], consequently, we chose to determine the biological activity of [Aβ(1–40)]$_{DiY}$ by comparing its ability to inhibit LTP with that of Aβ(1–40). The precise assembly form(s) of Aβ that cause neuronal compromise in AD are, as yet, ill-defined [3,7]. Thus rather than studying a single Aβ assembly, we collected peptide samples at defined time points along the aggregation reaction. In this way, we compared the synaptic plasticity disrupting activity of unaggregated and mixed aggregates of each peptide. For Aβ(1–40) and [Aβ(1–40)]$_{DiY}$, mixed aggregates were prepared using SEC to isolate peptides in 20 mM phosphate buffer, pH 8.0, and shaking the isolated material until they attained $t_{½max}$ (Figures 2A and 2B). Zero time ($t = 0$) and $t_{½max}$ samples were flash frozen and stored at −80 °C. Aliquots of these were then thawed immediately before biophysical or electrophysiology experiments. The most prominent assemblies present in the $t_{½max}$ Aβ(1–40) sample are clumped stunted fibrils (length, 151 ± 54 nm; width, 10 ± 2 nm), whereas $t_{½max}$ [Aβ(1–40)]$_{DiY}$ samples contain a heterogeneous mixture of both individual short smooth fibrils (length, 43 ± 19 nm; width, 7 ± 1 nm) and longer ribbon-like fibrils (length, 200 ± 192 nm; width, 11 ± 1 nm) with periodic twist (periodicity ∼200 nm) (Supplementary Figures S4A and S4B). In keeping with the clumped structures detected by EM, analytical SEC reveals that the aggregates present in $t_{½max}$ Aβ(1–40) samples are removed by centrifugation (at 16000 ***g*** for 30 min) and the only soluble species remaining is Aβ monomer, the latter accounting for only approximately one-third of the starting Aβ monomer amount (Supplementary Figure S6D at http://www.biochemj.org/bj/461/bj4610413add.htm). In contrast, the short smooth fibrils in $t_{½max}$ [Aβ(1–40)]$_{DiY}$ do not readily form sediment, and elute in the void volume of the SEC column (Supplementary Figure S6E). As a positive control, [Aβ(1–40)S26C]$_2$ was prepared as reported previously [17] (Figure 2C). Such preparations contain small protofibril-like species (length, 42 ± 12 nm; width, 7 ± 1 nm), the bulk of which remain in solution following centrifugation (Supplementary Figures S6C and S6F).

We then tested the effects of unaggregated ($t = 0$) and mixed aggregates ($t_{½max}$) of Aβ(1–40) and [Aβ(1–40)]$_{DiY}$ on excitatory synaptic transmission in the anaesthetized rat hippocampus. Since we already knew that soluble aggregates of [Aβ(1–40)S26C]$_2$ can block LTP [17], the goal of this experiment was to determine whether: (i) authentic low-molecular-mass [Aβ(1–40)]$_{DiY}$; and/or (ii) soluble aggregates of [Aβ(1–40)]$_{DiY}$ inhibit LTP. Owing to the complexity regarding relative concentrations of active species, these experiments do not address relative potency. An intracerebroventricular injection of 160 pmol (in 8 μl) of each $t_{½max}$ sample at 15 min before HFS inhibits LTP to a similar extent {105.9 ± 1.5 %, $n = 5$, and 109.2 ± 2.2 %, $n = 6$, for Aβ(1–40) and [Aβ(1–40)]$_{DiY}$ respectively, $P < 0.05$ compared with 129.6 ± 1.7 %, $n = 8$ in vehicle injected controls; $P > 0.05$ compared with each other} (Figure 2D). In contrast, neither unaggregated Aβ(1–40) monomer nor [Aβ(1–40)]$_{DiY}$ alters LTP (160 pmol, 126.0 ± 3.0 %, $n = 4$, and 124.7 ± 2.6 %, $n = 6$, respectively, $P > 0.05$), with LTP being indistinguishable from that in the vehicle control (Figure 2D). In accordance with our previous study, [Aβ(1–40)S26C]$_2$ protofibrils at this dose also strongly inhibited LTP (114.3 ± 1.2 %, $n = 7$, $P \leqslant 0.05$ compared with vehicle) [17]. The dose of 160 pmol of Aβ was chosen because it caused near-maximum inhibition of LTP (Figure 2D).

These data demonstrate that similar to [Aβ(1–40)S26C]$_2$, [Aβ(1–40)]$_{DiY}$ and Aβ(1–40) can aggregate to form assemblies that are potent synaptotoxins, whereas the unaggregated monomer and [Aβ(1–40)]$_{DiY}$ do not affect LTP. The lack of effect of [Aβ(1–40)]$_{DiY}$ on LTP is in keeping with our previous demonstration that [Aβ(1–40)S26C]$_2$ does not alter LTP [17], and suggests that

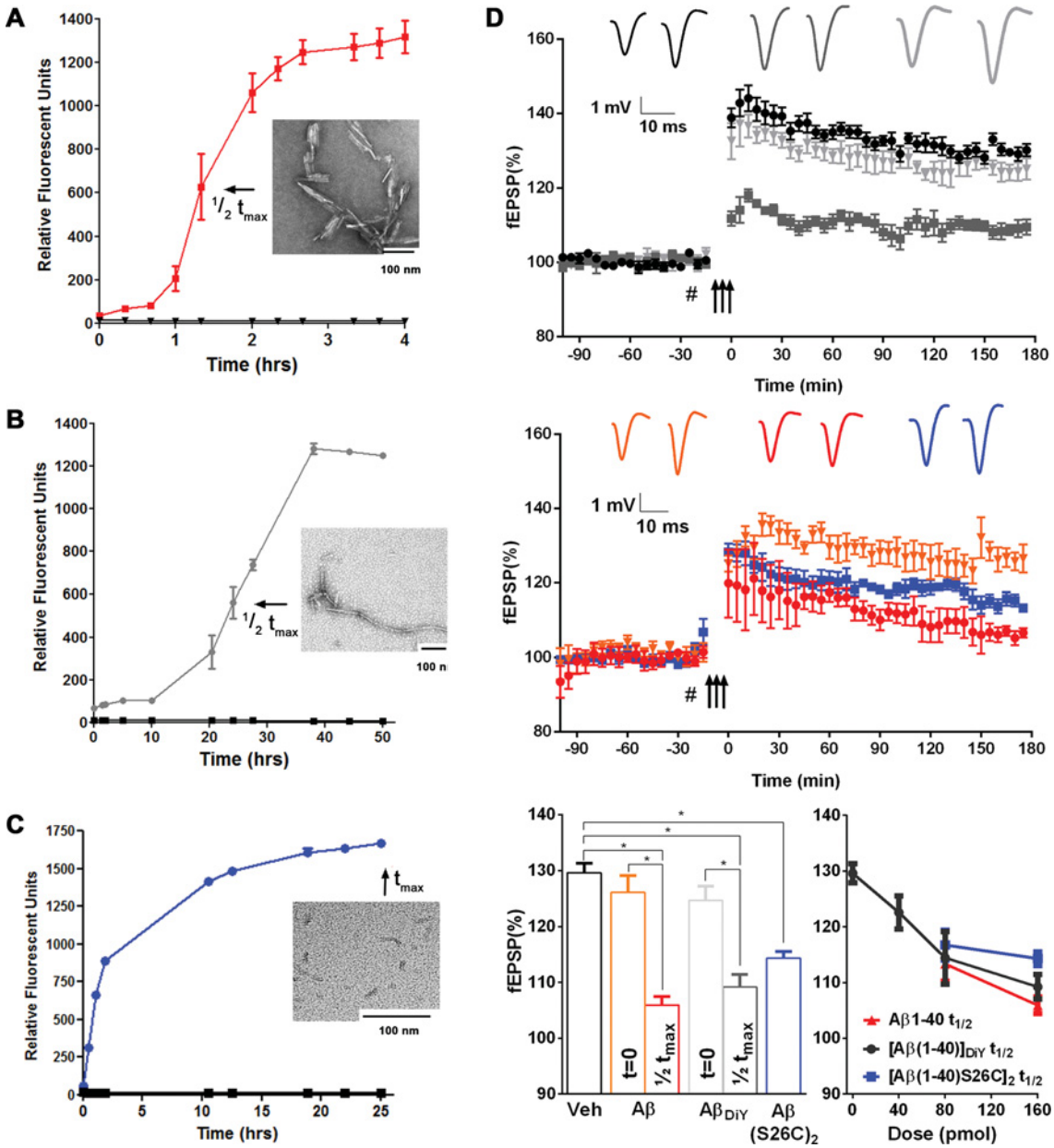

Figure 2 Aggregated Aβ(1–40), [Aβ(1–40)]$_{DiY}$ and [Aβ(1–40)S26C]$_2$ impair *in vivo* LTP in rats

(**A**–**C**) Peptide aggregation monitored by ThT fluorescence. All peptides were SEC-isolated in 20 mM sodium phosphate, pH 8.0, and incubated at 37 °C in the absence or presence of ThT. Aβ(1–40) (red) and [Aβ(1–40)]$_{DiY}$ (grey) were incubated with shaking and [Aβ(1–40)S26C]$_2$ (blue) without shaking. Aliquots were taken at $t = 0$, $t_{1/2max}$ or t_{max}, flash frozen and stored at − 80 °C until use. (**D**) In control animals injected intracerebroventricularly (#) with vehicle (Veh) (8 μl, black circles), the application of HFS (↑↑↑) induced robust LTP. In the case of [Aβ(1–40)]$_{DiY}$ (160 pmol), the $t_{1/2max}$ preparation (dark grey squares) strongly inhibited LTP, whereas the $t = 0$ sample (light grey triangles) had no significant effect on the magnitude of LTP. Similarly, injection of 160 pmol of $t_{1/2max}$ Aβ(1–40) (red circles), but not the $t = 0$ Aβ(1–40) monomer sample (160 pmol, orange triangles), strongly inhibited LTP. [Aβ(1–40)S26C]$_2$ protofibrils (160 pmol, blue squares) also caused a robust inhibition of LTP. Insets show representative EPSP traces during the last 10 min of baseline and last 10 min of the recording. Data for the magnitude of LTP measured at 3 h after the HFS in all treatment groups are summarized in the histogram. As shown in the dose–response graph ($n = 4$–8 per dose), this dose (160 pmol) of all three preparations caused near-maximum inhibition of LTP at this time. Values are the mean ± S.E.M. *$P < 0.05$. fEPSP, field EPSP.

the plasticity disrupting activity previously attributed to brain-derived dimers [10,16] is mediated not by the dimers, but by the higher assemblies the dimers form. It is intriguing that all three peptides form toxic assemblies, despite the distinct morphologies of their aggregates. In an effort to better understand the basis of the dramatically different aggregation kinetics and assembly forms that these peptides produced, we investigated the structures of the component monomers and dimers.

Recombinantly produced and chemically synthesized Aβ peptides have similar aggregation kinetics and products

The method of choice for high-resolution analysis of protein and peptide structure is NMR spectroscopy, a method which necessitates the use of isotopically labelled (^{13}C and ^{15}N) peptides. Recombinant ^{13}C- and ^{15}N-labelled Aβ wild-type and S26C peptides (see below) contain an exogenous N-terminal

methionine residue [27], thus we were careful to compare the aggregation of recombinant Aβ(M1–40), [Aβ(M1–40)]$_{DiY}$ and [Aβ(M1–40)S26C]$_2$ with that of chemically synthesized Aβ(1–40), [Aβ(1–40)]$_{DiY}$ and [Aβ(1–40)S26C]$_2$. All three recombinant peptides aggregated in a manner similar to their synthetic counterparts (compare Figure 1 with Supplementary Figure S7 at http://www.biochemj.org/bj/461/bj4610413add.htm), but as reported previously, recombinant peptides (presumably because of their greater molecular purity) aggregate faster than their synthetic counterparts. Nonetheless, the rank order of aggregation was the same. For instance, at 20 μM, Aβ(M1–40) and Aβ(1–40) have similar aggregation rates (19.1 RFU/min compared with 15.5 RFU/min) and both peptides form a meshwork of laterally associated fibrils (compare Figure 1D with Supplementary Figure S7C). [Aβ(M1–40)]$_{DiY}$ and [Aβ(1–40)]$_{DiY}$ exhibit similarly long lag phases (<4 h) and low-aggregation rates (3.2 RFU/min compared with 1.1 RFU/min) and form very long smooth fibrils of ∼10 nm in diameter (Figure 1 compared with Supplementary Figure S7). The aggregation profile of chemically synthesized [Aβ(1–40)S26C]$_2$ and recombinantly expressed [Aβ(M1–40)S26C]$_2$ are also similar with each aggregating without a lag and forming short thick fibrils (Figure 1 and Supplementary Figure S7).

Mild alkaline pH and low temperature prevents aggregation of Aβ(M1–40), [Aβ(M1–40)]$_{DiY}$ and [Aβ(M1–40)S26C]$_2$ and facilitates analysis of authentic monomer and dimers

Having assured ourselves that recombinant and synthetic peptides aggregate in a similar manner, we then proceeded to investigate conditions that would allow isolation and use of highly concentrated recombinant peptide samples, yet would preclude aggregation over the 2 h period required for NMR experiments. To achieve this, we used 25 mM ammonium bicarbonate buffer at pH 8.0. In order to simulate conditions to be used for NMR, we tested peptide samples collected into NMR tubes immediately after SEC isolation and again following 2 h of incubation at 4 °C. Analytical SEC indicated that even after 24 h monomer and dimers did not assemble further (Figure 3A). Although there were no indications of higher-molecular-mass species, it is possible that certain Aβ aggregates could stick to the column. To control for this possibility, we monitored the height and area of monomeric/dimeric peaks. Using this approach we could discern no change in the amount of Aβ(M1–40) monomer or [Aβ(M1–40)]$_{DiY}$ (Figure 3A). In contrast, there was a ∼4 % reduction in the amount of [Aβ(M1–40)S26C]$_2$ detected at 24 h compared with $t = 0$, but importantly, there was no reduction after 2 h (Figure 3A, inset).

To complement our SEC analysis, we also used a solution-based non-invasive technique, QLS, which revealed that SEC-isolated Aβ(M1–40) had a R_H of ∼1.7 nm, whereas the R_H for both [Aβ(M1–40)]$_{DiY}$ and [Aβ(M1–40)S26C]$_2$ was ∼2.2 nm (Figure 3B, panel i). These estimates are consistent with the expected size of Aβ monomer and dimers. Since the intensity of light scattered by a particle is proportional to its mass squared, and assuming at the least a linear dependence of the R_H on the particle mass, we conservatively estimate that ⩾99 % of Aβ(M1–40) existed as monomer and that ⩾99 % of [Aβ(M1–40)]$_{DiY}$ and [Aβ(M1–40)S26C]$_2$ existed as dimers. Furthermore, analysis of the same samples at 2 h following SEC isolation (incubated at 4 °C; Figure 3B, panel ii) and then continuously for a further 22 h (Figure 3B, panel iii), revealed that only trace amounts (⩽0.1 % of total Aβ) of higher-molecular-mass species formed during the time course studied. The concentration of the aggregates estimated by QLS is so low that it would not influence the results of either CD or NMR spectroscopy.

The secondary structure of [Aβ(M1–40)]$_{DiY}$ and [Aβ(M1–40)S26C]$_2$ differ subtly from each other and from Aβ monomer

As seen previously, CD analysis of SEC-isolated Aβ(1–40) detected little or no secondary structure [31]. SEC-isolated [Aβ(M1–40)]$_{DiY}$ and [Aβ(M1–40)S26C]$_2$ produced spectra that were similar to Aβ(M1–40) (Figures 4A and 4B). There is a slight shift in the minimum of [Aβ(M1–40)]$_{DiY}$ (199 nm) compared with Aβ(M1–40) (201 nm), probably a result of differences in the spectral properties of tyrosine and DiY [44]. The minimum of [Aβ(M1–40)S26C]$_2$ corresponds with that of Aβ(M1–40) (both at 201 nm), however, it is slightly less pronounced. Importantly, there are no differences between the three peptides in the regions most associated with β-sheet (212–218 nm) or α-helix (208 nm, 222 nm) [45] and both [Aβ(M1–40)]$_{DiY}$ and [Aβ(M1–40)S26C]$_2$ exhibit maxima at ∼195 nm.

We used NMR spectroscopy to search for local secondary structure differences that would not be detected by CD. A battery of NMR analyses (Table 1) allowed a near complete backbone assignment for Aβ(M1–40), [Aβ(M1–40)]$_{DiY}$ and [Aβ(M1–40)S26C]$_2$. Aβ(M1–40) is highly disordered, as indicated by narrow cross-peaks for all residues. 2D aliphatic (^{13}C,^{1}H)-HSQC spectra for [Aβ(M1–40)]$_{DiY}$ and [Aβ(M1–40)S26C]$_2$ largely overlap with that of Aβ(M1–40) (Figures 4C and 4D). ^{13}C,^{1}H cross-peak differences between the dimers and wild-type monomer are mainly located around the sites of covalent cross-linking (Figures 4C and 4D) and ^{13}Cα,^{1}Hα cross-peak intensities are decreased in these regions (Supplementary Figure S8 at http://www.biochemj.org/bj/461/bj4610413add.htm). The major differences between Aβ(M1–40) and [Aβ(M1–40)]$_{DiY}$ occur at Ser^{8}, Gly^{9}, Tyr^{10}, Glu^{11}, Val^{12} and His^{13}. In contrast the principal differences between [Aβ(M1–40)S26C]$_2$ and Aβ(M1–40) are at Val^{24}, Gly^{25} and Asn^{27}. Tyr^{10} in [Aβ(M1–40)]$_{DiY}$ does not register as a result of restricted movement due to cross-linking of the tyrosine residues. Similarly, no signal for Cys^{26} was registered in [Aβ(M1–40)S26C]$_2$ due to reduced backbone mobility.

Since ^{1}Hα, ^{13}Cα and ^{13}CO chemical shifts are extremely sensitive to secondary structure [46], we first used these to gauge whether any changes in secondary structure might have resulted from covalent dimerization that could explain differences in aggregation kinetics and/or the types of aggregates formed. Figures 5(A)–5(C) shows the extracted backbone ^{1}Hα, ^{13}Cα and ^{13}CO chemical shifts for [Aβ(M1–40)]$_{DiY}$ minus the chemical shift signal for the equivalent residue in Aβ(M1–40) monomer, whereas Figures 5(D)–5(F) shows the same analysis for [Aβ(M1–40)S26C]$_2$. The observed chemical shift changes are relatively modest (<0.1 p.p.m. for ^{1}H and <0.3 p.p.m. in the case of ^{13}C, barring a single exception). These results are in keeping with our CD analysis and indicate that no major overall structural conversions occurred (Figure 4). This fact notwithstanding, NMR chemical shift differences observed between the samples are significant, and also distinct for the two dimeric peptides. In [Aβ(M1–40)]$_{DiY}$, we see negative values for the change in ^{1}Hα chemical shift, coupled with increases in ^{13}Cα and ^{13}CO chemical shifts, and this is restricted around the region of cross-linking (residues His^{6}–Val^{12}). [Aβ(M1–40)S26C]$_2$ chemical shift differences are similarly weak, however, in contrast with those of [Aβ(M1–40)]$_{DiY}$, [Aβ(M1–40)S26C]$_2$ exhibits opposite values for ^{1}Hα, ^{13}Cα and ^{13}CO chemical shift changes, indicating an opposite trend in its inclination for secondary structure. In addition, these changes are observed on either side of the disulfide

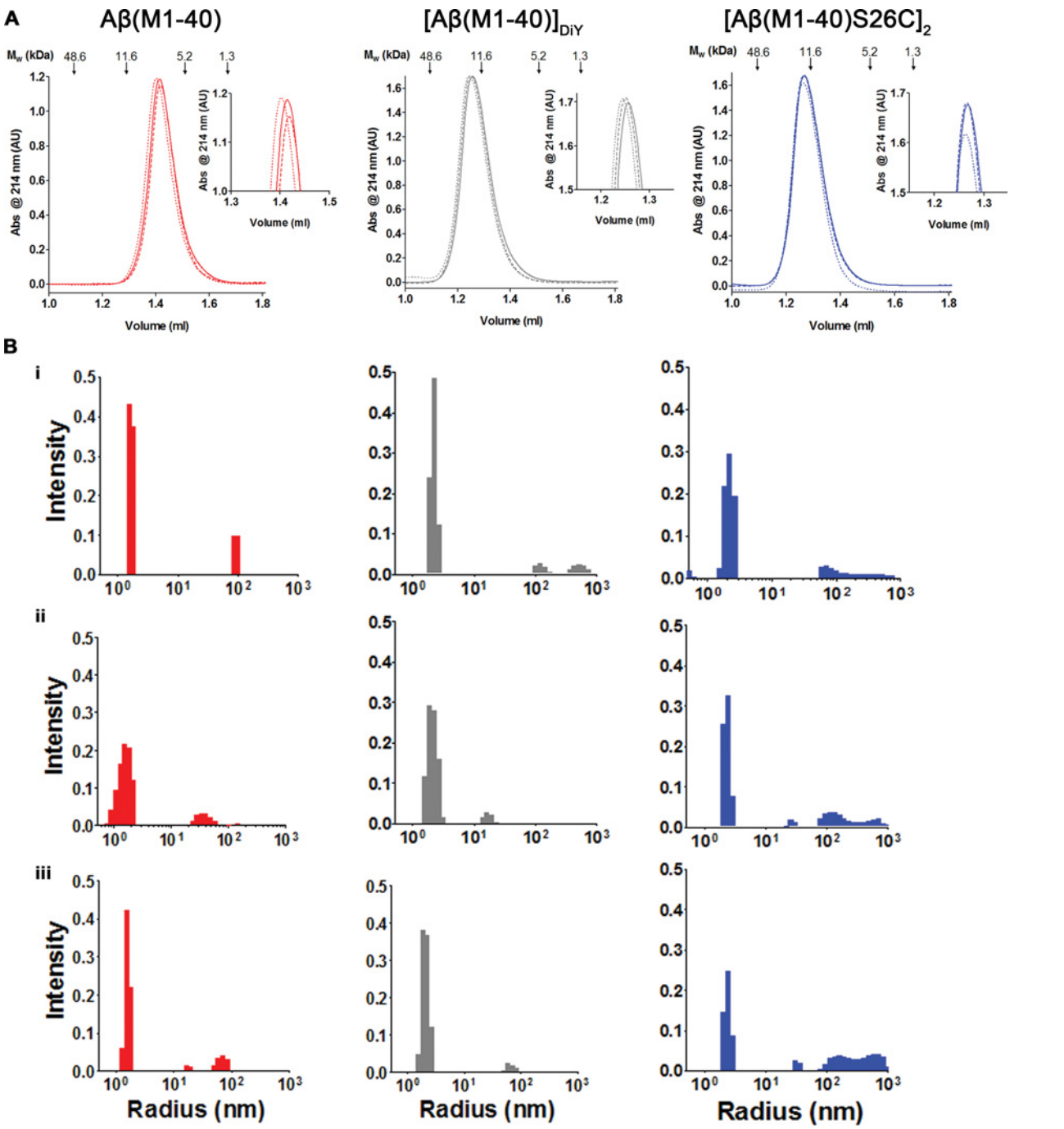

Figure 3 Concentrated solutions of Aβ(M1–40), [Aβ(M1–40)]$_{DiY}$ and [Aβ(M1–40)S26C]$_2$ in 25 mM ammonium bicarbonate, pH 8.0, show little propensity for aggregation

Aβ(M1–40) (red), [Aβ(M1–40)]$_{DiY}$ (grey) and [Aβ(M1–40)S26C]$_2$ (blue) were isolated by SEC in 25 mM ammonium bicarbonate, pH 8.0, to produce samples of ~200 μM and analysed by analytical SEC and QLS. (**A**) At 0 h (continuous line), 2 h (dashed line) and 24 h (dotted), 10 μl of each ~200 μM solution was injected on to a Superdex 75 SEC column and eluted at 0.05 ml/min in 25 mM ammonium bicarbonate, pH 8.0. Elution of linear dextran standards is indicated by arrows. Expanded views reveal that the amount of Aβ(1–40) and [Aβ(1–40)]$_{DiY}$ remained constant throughout the time course, whereas after 24 h there was a very slight decrease in [Aβ(M1–40)S26C]$_2$. (**B**) Aβ(M1–40), [Aβ(M1–40)]$_{DiY}$ and [Aβ(M1–40)S26C]$_2$ were isolated from SEC directly into QLS cuvettes and analysed within (**B**, panel i) 2 min of collection, (**B**, panel ii) at 2 h following incubation at 4 °C and (**B**, panel iii) again at 24 h.

cross-link, and extend also further away, affecting the structural propensity of residues Leu^{17}–Phe^{20} and Leu^{34}–Gly^{37} (Figures 5D–5F).

To better appreciate the exact extent of structural change, we next converted the observed chemical shifts for Aβ(M1–40), [Aβ(M1–40)]$_{DiY}$ and [Aβ(M1–40)S26C]$_2$ into absolute propensities to form an α-helix or β-strand at each position in the primary sequence. This is done by calculating the difference $\Delta\delta$ between the observed chemical shifts and those expected for 'random coil' values of the same polypeptide. For ^{1}Hα, positive values then signify β-sheet propensity, whereas negative shifts denote helical propensity. Analogously, for ^{13}Cα and ^{13}CO,

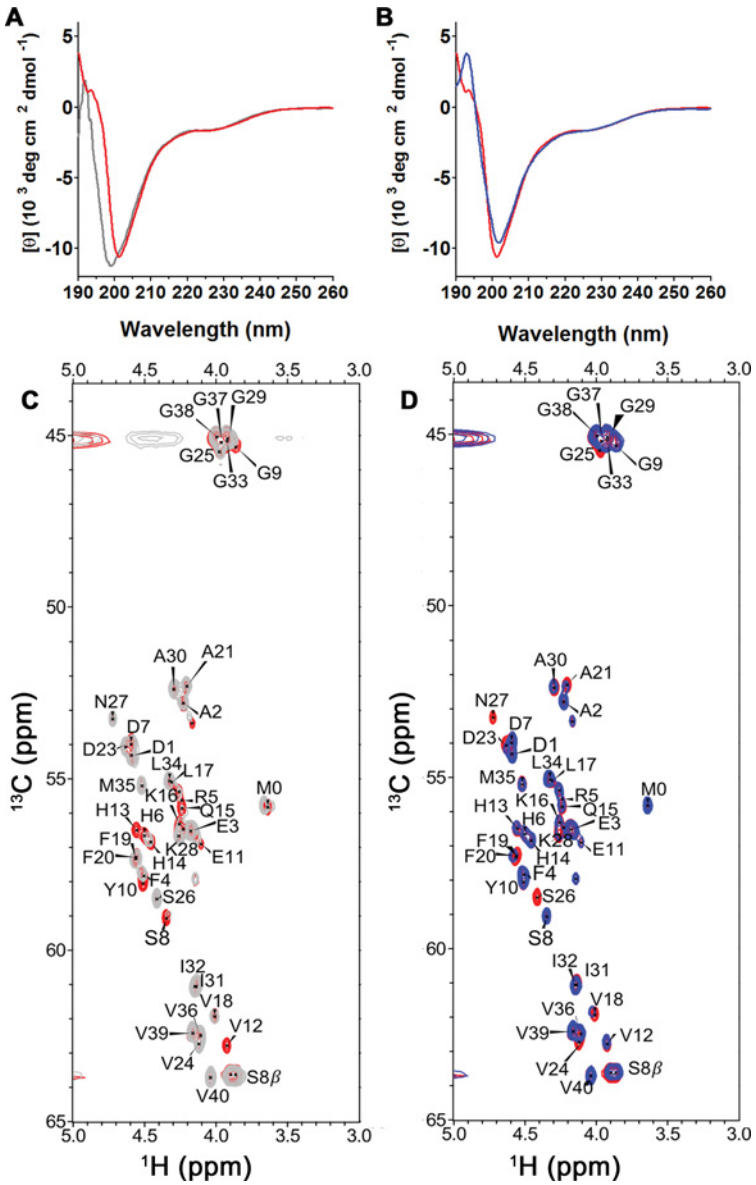

Figure 4 Overlay of CD and 2D NMR spectra for Aβ(M1–40) with $[Aβ(M1–40)]_{DiY}$ and $[Aβ(M1–40)S26C]_2$

Peptides were SEC-isolated at ~200 μM in 25 mM ammonium bicarbonate, pH 8.0, and used immediately. For CD, samples were diluted to 0.45 mg/ml and spectra of (**A**) Aβ(M1–40) (red) with $[Aβ(M1–40)]_{DiY}$ (grey), and (**B**) Aβ(M1–40) (red) with $[Aβ(M1–40)S26C]_2$ (blue) are shown. 2D (^{13}C,^{1}H)-HSQC NMR spectra were recorded from SEC-isolated ^{13}C,^{15}N-labelled Aβ(M1–40), $[Aβ(M1–40)]_{DiY}$ and $[Aβ(M1–40)S26C]_2$. The Cα,Hα signals for (**C**) $[Aβ(M1–40)]_{DiY}$ (grey) are overlaid on Aβ(M1–40) (red) and (**D**) $[Aβ(M1–40)S26C]_2$ (blue) overlaid on Aβ(M1–40) (red). All peaks are annotated with the single letter amino acid code and their position in the sequence. Broad features present in the spectrum around 45 p.p.m. and 64 p.p.m. (^{13}C chemical shift) result from incomplete suppression of the water signal.

negative values correspond to β-sheet propensity and positive differences equate to α-helix propensity [46]. In what follows, 'random coil' reference values are taken from a neighbour-corrected random coil chemical shift library for intrinsically disordered protein sequences [37,38].

Subsequently, the program ncSPC was used to predict adoption of canonical secondary structure conformations (i.e. α-helix or β-sheet) on a continuous scale from 0 to 1 [37,38]. Using this approach, Aβ(M1–40) is predicted to contain two regions of helical propensity. The first involves a relatively long stretch between residues His^6–Lys^{16} and the second a short stretch between residues Gly^{38}–Val^{40}. But the strongest predicted feature indicates two backbone regions prone to forming β-sheet secondary structure, between residues Val^{17}–Val^{24} and Ala^{30}–Met^{35} (Figure 6A). These are the same regions known to form in an anti-parallel β-sheet when Aβ(1–40) is complexed with the single-chain affibody, $ZAβ_3$ [47], and to participate in the intermolecular β-sheets formed by Aβ monomers stacked along the long axis of fibrils (reviewed in [48]). The introduction of a covalent cross-link between tyrosine residues in $[Aβ(1–40)]_{DiY}$ yields a large increase in the predicted helical propensity between residues Glu^3–Val^{12} and a loss of helicity in the C-terminus involving residues Gly^{38}–Val^{40} (compare Figures 6A and 6B). Otherwise $[Aβ(M1–40)]_{DiY}$ and Aβ(M1–40) are highly similar. In contrast, $[Aβ(M1–40)S26C]_2$ has a notably increased propensity for β-sheet formation with small, but observable,

Table 1 Complete list of NMR measurements

Experiment	Number of scans	Nucleus	Spectral width (Hz)	Carrier position (p.p.m.)	Maximum evolution time (ms)	Total experimental time
(^{15}N,^{1}H)-HSQC	16	^{15}N	1650	119.288	77.6	1 h 17 min
		^{1}H	8000	5.028	64	
(^{13}C,^{1}H)-HSQC	8	^{13}C	10000	43.3261	20	1 h 15 min
		^{1}H	8000	5.028	64	
2D CO(CA)H	32	^{13}C	1500	174	133	7 h 55 min
		^{1}H	8000	5.028	64	
2D HA(CA)N	84	^{1}H	8000	5.028	64	7 h 43 min
		^{15}N	1650	119.28	85	
3D HNCO	8	^{1}H	8000	5.028	64	16 h 19 min
		^{15}N	1650.01	119.28	24.2	
		^{13}C	1500	176.251	26	
3D HNCA	8	^{1}H	8000	5.028	64	16 h 17 min
		^{15}N	1650	119.28	24.2	
		^{13}C	3920	56	10	
1D	128	^{1}H	8000	5.028	1	5 min

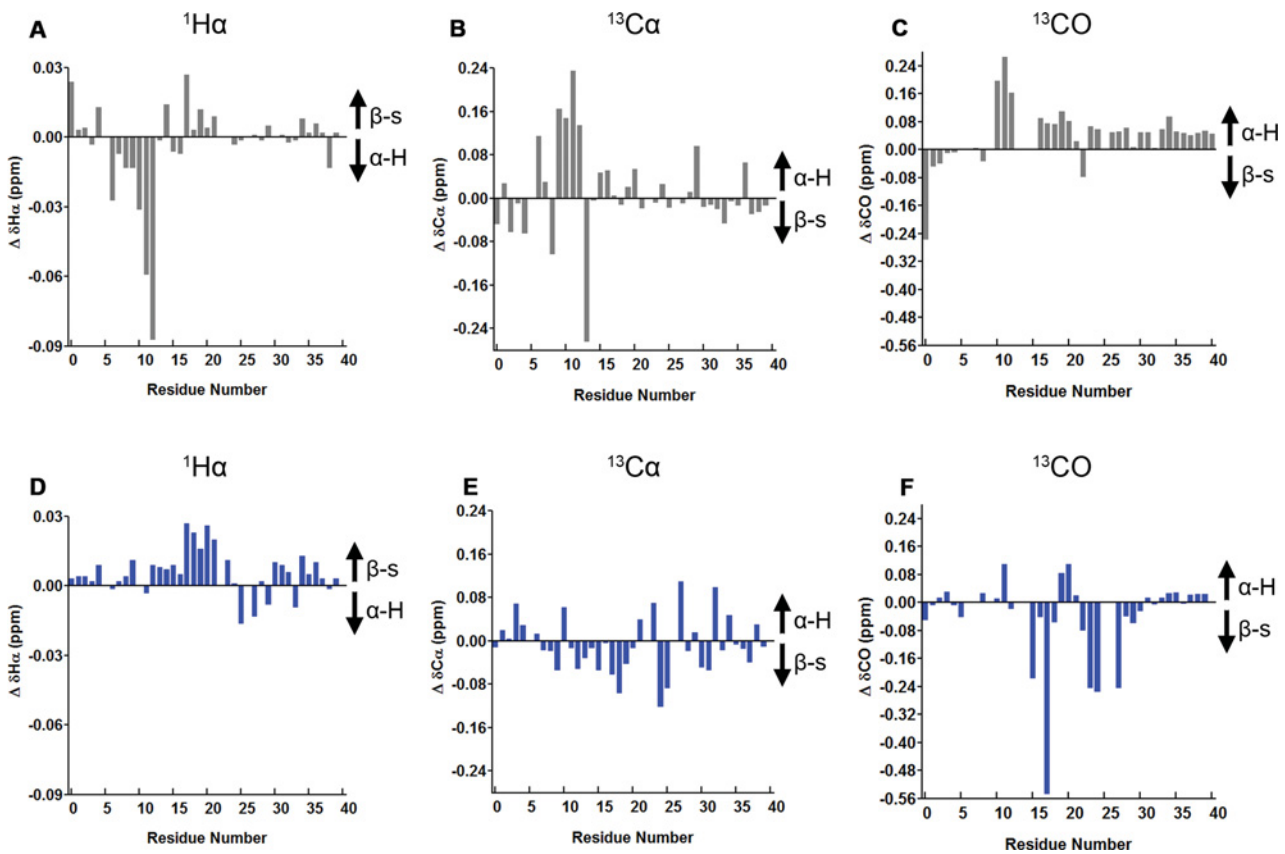

Figure 5 Covalent cross-links in Aβ dimers cause small, but specific, changes to local and global 2D structures

Chemical shift differences ($\Delta\delta$) observed for (**A** and **D**) ^{1}Hα, (**B** and **E**) ^{13}Cα and (**C** and **F**) ^{13}CO at pH 8.0, comparing (**A**–**C**) [Aβ(M1–40)]$_{DiY}$ with Aβ(M1–40) and (**D**–**F**) [Aβ(M1–40)S26C]$_2$ with Aβ(M1–40). Chemical shift differences between Aβ(M1–40)$_{DiY}$ and Aβ(M1–40) are calculated as $\Delta\delta = \delta$[Aβ(M1–40)]$_{DiY}$ $- \delta$[Aβ(M1–40)]; chemical shift differences between [Aβ(M1–40)S26C]$_2$ and Aβ(M1–40) are calculated as $\Delta\delta = \delta$[Aβ(M1–40)S26C]$_2$ $- \delta$[Aβ(M1–40)]. For ^{1}Hα, positive differences indicate increased β-sheet formation and/or reduced helical propensity, whereas negative differences denote the opposite. For ^{13}Cα and ^{13}CO spectra, the opposite is the case, positive differences indicate increased helical structure and reduced β-sheet formation, whereas negative shifts correspond to the opposite situation.

increases in predicted β-sheet propensity within residues Gln^{15}–Gly^{25} and Asn^{27}–Ile^{32}, and to a lesser extent Gly^{38}–Val^{40} (compare Figures 6A and 6C). When analysed using ncSPC, the Aβ(1–40)–ZAβ3 complex reported by Hoyer et al. [47] (Supplementary Figure S9 at http://www.biochemj.org/bj/461/bj4610413add.htm) showed the involvement of the same residues in β-sheet propensity. Given this is a very stable complex, the predicted β-sheet propensity is extremely high. These results demonstrate that covalent cross-links between monomers have a modest, but detectable, influence on the secondary structure propensity of Aβ.

Overall, the [Aβ(M1–40)]$_{DiY}$ cross-linked peptide is associated with a slight increase in helicity throughout the Aβ molecule,

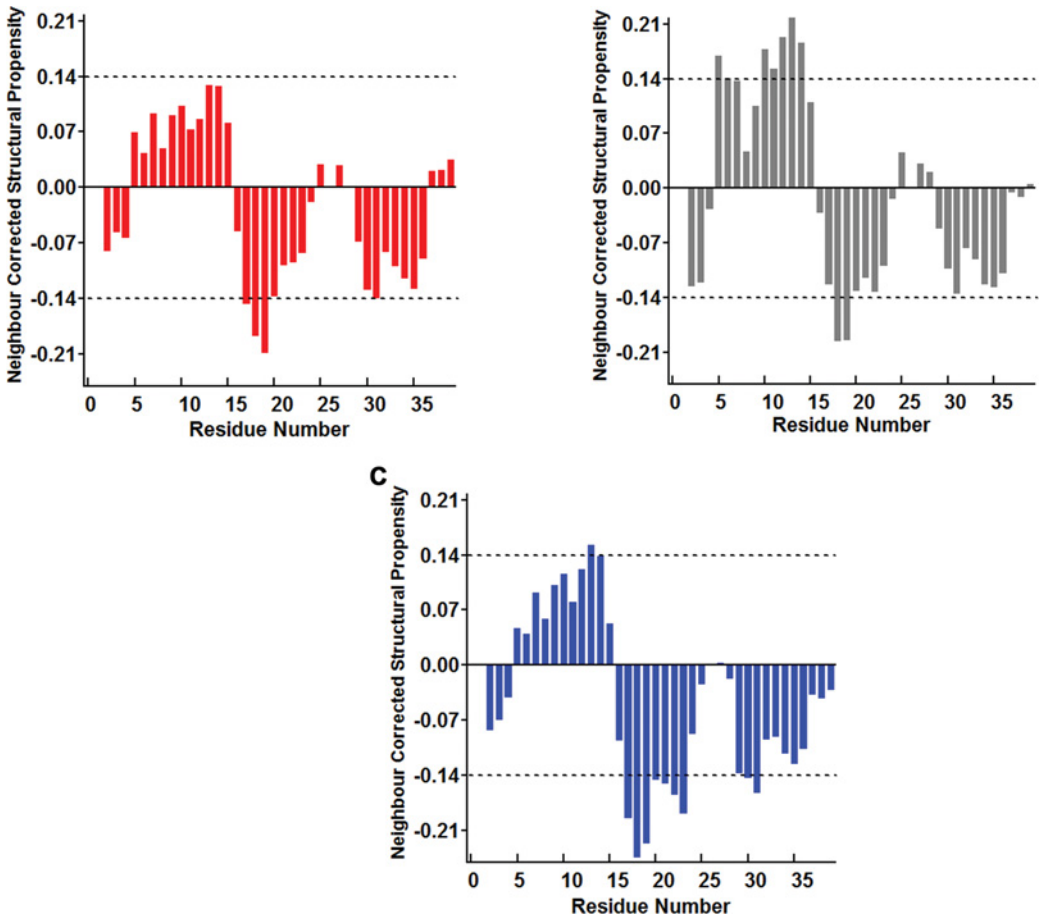

Figure 6 Covalently cross-linked $[A\beta(M1–40)]_{DiY}$ and $[A\beta(M1–40)S26C]_2$ are intrinsically disordered and exhibit small differences in secondary structure propensity relative to Aβ(M1–40)

Structural propensity of (**A**) Aβ(M1–40), (**B**) $[A\beta(M1–40)]_{DiY}$ and (**C**) $[A\beta(M1–40)S26C]_2$ at pH 8.0 based on $^{13}C\alpha$, $^{1}H\alpha$, ^{15}N and $^{13}C'$ backbone chemical shifts. The structural propensity for each chemical shift was calculated using ncSPC [38]. Positive values indicate helical propensity and negative values predict β-sheet conformation. Broken lines at 0.14 and −0.14 are included for ease of comparison.

except at the extreme C-terminus, and this dimer aggregates very slowly forming long smooth fibrils. In contrast, the cystine cross-link produces a dimer that aggregates extremely rapidly, but only forms short fibrils. On basis of the collective data presented, it is apparent that rather modest differences in the secondary structure propensity have a drastic influence on the type and rate at which aggregates are formed.

DISCUSSION

Considerable evidence suggests that dimers of Aβ play an important role in AD [8,10,16,28,49–52], however, owing to the low abundance and difficulty in purifying native dimers, their structure and aggregation propensity have not been investigated. In Nature, there are few possible ways by which covalent dimers could be formed, the most likely of which involve the coupling of two Aβ monomers by a DiY bond, $[A\beta]_{DiY}$. Thus we studied $[A\beta]_{DiY}$, and for comparison, we also investigated the previously described design dimer, $[A\beta S26C]_2$ [17]. In their unaggregated state, $[A\beta]_{DiY}$ and $[A\beta S26C]_2$ lack appreciable structure and fail to alter LTP. However, both dimers self-associate to form larger structures and during the assembly process generate aggregates that potently block LTP. These data have important implications for our understanding of AD, in that contrary to previous assertions, dimers themselves are not directly toxic. Moreover, the lack of stable structure in the starting dimers indicates that differences in aggregation propensities of $[A\beta]_{DiY}$ and $[A\beta S26C]_2$ are not driven by fixed structures in these dimers, but by the population of structures that dimers can access, and by how well certain dimer structures can be accommodated into the quaternary structure of protofibrils and fibrils.

Recent work indicates that aggregation of Aβ monomer involves both primary and secondary nucleation [53,54], and that aggregation under agitated conditions is enhanced by breakage of fibrils to form new seeds [55]. Primary nucleation occurs first and involves only monomer. The nuclei thus formed grow quickly and fibrils appear. Thereafter fibrils provide a catalytic surface for nucleation from monomers, and secondary nucleation becomes faster than primary nucleation [53,54]. Even at high concentrations $[A\beta]_{DiY}$ has a lag phase more than 20-fold as long and an aggregation rate ∼15-fold lower than found for equivalent concentrations of Aβ monomer. Thus the DiY cross-link seems to inhibit primary nucleation and subsequently retards fibril elongation and fibril–fibril interactions. The fibrils formed by $[A\beta]_{DiY}$ are remarkable in their long length and consistent

morphology, features which indicate that $[A\beta]_{DiY}$ fibrils are highly stable and well-ordered. It is interesting to speculate how the aggregation of $[A\beta]_{DiY}$ relates to its structural propensity. Tyr^{10} lies in an unstructured region outside the β-hairpin found in the core of amyloid fibrils [56–58], SDS-stabilized oligomers [59] or Aβ monomer complexed with the affibody, $ZA\beta_3$ [47]. Our chemical shift analysis indicates that dimer formation at Tyr^{10} leads to an overall increase in the helical propensity of residues Arg^5–Gln^{15}, but has little effect on β-sheet forming residues. Thus the slower kinetics and more regular fibrils formed by $[A\beta]_{DiY}$ may result not from differences in propensity to form β-sheets, but rather from differences in the type of β-sheets formed. For instance, the increased helicity in the N-terminus and the modest increase in β-sheet propensity of Gly^{37}–Gly^{38} could promote intermolecular parallel β-sheets favoured by mature fibrils [56–58]. In future studies, it will be important to use solid-state NMR to investigate the structure of $[A\beta]_{DiY}$ fibrils, and of fibrils formed from mixtures of Aβ monomer and of $[A\beta]_{DiY}$.

In contrast with $[A\beta]_{DiY}$, $[A\beta S26C]_2$ goes immediately from a structure-poor dimer to an ordered aggregate capable of binding ThT, but shows slower post-lag aggregation than the Aβ monomer. This suggests that the disulfide bond at residue 26 acts to accelerate nucleation or that $[A\beta S26C]_2$ itself serves as a nucleus. In either case, the consequence is to retard fibril elongation and fibril–fibril interactions. This is in keeping with our previous report that $[A\beta S26C]_2$ forms kinetically trapped protofibrils [17]. Moreover, the enhancement of nucleation seen in $[A\beta S26C]_2$ relative to Aβ monomer is congruent with the subtle structural differences revealed by our comparison of chemical shift differences and suggest that $[A\beta S26C]_2$'s faster nucleation results from an increased propensity to form β-structure. In previous studies, intramolecular disulfide cross-links engineered to stabilize a two-stranded anti-parallel β-sheet produced an Aβ monomer (referred to as Aβcc) that readily formed protofibrils, but that was incapable of forming fibrils [60]. Since the disulfide link in $[A\beta S26C]_2$ is intermolecular and is positioned within the proposed bend/turn found in both amyloid fibrils [56–58] and Aβcc [47,60], the increased β-propensity of $[A\beta S26C]_2$ could lead to formation of either intramolecular anti-parallel β-sheets or intermolecular parallel β-sheets. Indeed, solution NMR studies of oligomers formed in the presence of SDS found both inter- and intra-molecular β-sheets [59]. Given the predicted increase in β-sheet propensity of residues Leu^{17}–Gly^{25} and Lys^{28}–Val^{39}, it is conceivable that $[A\beta S26C]_2$ assumes a conformation in protofibrils similar to that observed for dimer subunits in SDS-stabilized oligomers [59]. Conversion from this mixed anti-parallel/parallel conformation into the topologically distinct β-hairpin characteristic of amyloid fibrils [56–58] might suffer from a higher energetic barrier and could explain why $[A\beta S26C]_2$ forms protofibrils, but not fibrils.

Thermodynamically, the formation of a particular aggregate structure depends on the free energy of competing structures, but high-kinetic barriers that slow down the formation of more stable aggregates, such as amyloid fibrils, also play an important role. Thus effects on fibril nucleation, elongation and/or fibril–fibril interactions could influence the kinetic stability of structures in at least two different ways: (i) accelerated nucleation could lead to more growing nuclei and therefore lower monomer concentration and hence shorter assemblies and (ii) physical instability could limit the length of certain structures. Both of these possibilities could explain the rapid appearance and long persistence of short protofibril-like structures formed by $[A\beta S26C]_2$ and the slow appearance and formation of the exceptionally long and ordered fibrils formed by $[A\beta]_{DiY}$.

Although the structural propensity and aggregation of $[A\beta S26C]_2$ and $[A\beta]_{DiY}$ are quite different, they have a similar functional outcome in that they populate intermediate assemblies for an extended period. Importantly, the assemblies that are formed inhibit synaptic plasticity, this despite the fact that their aggregate intermediates have different morphologies. Thus these findings demonstrate that a range of structures can impair synaptic plasticity, and that the size and diffusibility of aggregates may be key to their synaptotoxic activity. Similarly, it is reasonable to expect that other conditions which enhance the population of certain assemblies, for instance subtle changes in the ratios of different alloforms of Aβ [61], would lead to disease. In this regard, factors that control the 'lifetime' of synaptotoxic assemblies will be critical determinants of their toxic effect. Indeed, studies which have examined oligomerization, aggregation and toxicity of different ratios of Aβ42/Aβ40 indicate that toxicity is greatest for mixtures of Aβ40/Aβ42 that increase the lifetime of oligomeric assemblies [62,63]. In the case of $[A\beta]_{DiY}$, the slowed kinetics of aggregation would lead to a protracted period during which soluble synaptotoxic assemblies are present. Therefore what appear as very subtle changes in structural propensity could in fact have a dramatic and detrimental effect on cognition. Given that oxidative cross-linking of tyrosine residues represent the most likely way to form covalently linked Aβ dimers and that there is immuno-EM evidence of Aβ and DiY co-localizing in human specimens [22], it will be important to search for soluble species of $[A\beta]_{DiY}$ in the brain and cerebrospinal fluid and to elucidate the mechanisms by which $[A\beta]_{DiY}$ is formed. Moreover, although we have focused on dimers formed from the most naturally abundant form of Aβ, Aβ(1–40), it will be important to extend these studies to include dimers built from the more disease-associated Aβ(1–42) [64]; and to explore the important issues of heterodimers and different ratios of Aβ40 and Aβ42 dimers [65].

AUTHOR CONTRIBUTION

Dominic Walsh conceived the project. Dominic Walsh, Frans Mulder, Michael Rowan, George Benedek and Sara Linse directed the research. Tiernan O'Malley, Nur Oktaviani, Dainan Zhang, Brian O'Nuallain and Aleksey Lomakin designed and conducted the experiments. All of the authors contributed to writing the paper.

FUNDING

This work was supported by the Foundation for Neurologic Diseases (to D.M.W.), The Netherlands Organization for Scientific Research [grant number VIDI 700.56.422 (to F.A.A.M.)], the Swedish Research Council [grant number 521-2013-3679 (to S.L.)], and Science Foundation Ireland [grant number 10/IN.I/B3001] and the Health Research Board of Ireland [grant number COEN/2011/11] (to M.J.R.).

REFERENCES

1 Hebert, L. E., Weuve, J., Scherr, P. A. and Evans, D. A. (2013) Alzheimer disease in the United States (2010–2050) estimated using the 2010 census. Neurology **80**, 1778–1783 CrossRef PubMed

2 Tanzi, R. E. (2012) The genetics of Alzheimer disease. Cold Spring Harb. Perspect. Med. **2**, 1–10 CrossRef

3 Benilova, I., Karran, E. and De Strooper, B. (2012) The toxic Aβ oligomer and Alzheimer's disease: an emperor in need of clothes. Nat. Neurosci. **15**, 349–357 CrossRef PubMed

4 Klein, W. I., Krafft, G. A. and Finch, C. E. (2001) Targeting small Aβ oligomers: the solution to an Alzheimer's disease conundrum? Trends Neurosci. **24**, 219–224 CrossRef PubMed

5 Selkoe, D. J. (1991) The molecular pathology of Alzheimer's disease. Neuron **6**, 487–498 CrossRef PubMed

6 Hardy, J. and Selkoe, D. J. (2002) The amyloid hypothesis of Alzheimer's disease: progress and problems on the road to therapeutics. Science **297**, 353–356 CrossRef PubMed

7 Walsh, D. M. and Teplow, D. B. (2012) Alzheimer's disease and the amyloid β-protein. Prog. Mol. Biol. Trans. Sci. **107**, 101–124 CrossRef

8 Klyubin, I., Betts, V., Welzel, A. T., Blennow, K., Zetterberg, H., Wallin, A., Lemere, C. A., Cullen, W. K., Peng, Y., Wisniewski, T. et al. (2008) Amyloid β protein dimer-containing human CSF disrupts synaptic plasticity: prevention by systemic passive immunization. J. Neurosci. **28**, 4231–4237 CrossRef PubMed

9 Lambert, M. P., Barlow, A. K., Chromy, B. A., Edwards, C., Freed, R., Liosatos, M., Morgan, T. E., Rozovsky, I., Trommer, B., Viola, K. L. et al. (1998) Diffusible, nonfibrillar ligands derived from $A\beta_{1-42}$ are potent central nervous system neurotoxins. Proc. Natl. Acad. Sci. U.S.A. **95**, 6448–6453 CrossRef PubMed

10 Shankar, G. M., Li, S., Mehta, T. H., Garcia-Munoz, A., Shepardson, N. E., Smith, I., Brett, F. M., Farrell, M. A., Rowan, M. J., Lemere, C. A. et al. (2008) Amyloid-β protein dimers isolated directly from Alzheimer's brains impair synaptic plasticity and memory. Nat. Med. **14**, 837–842 CrossRef PubMed

11 Kuo, Y. M., Emmerling, M. R., Vigo-Pelfrey, C., Kasunic, T. C., Kirkpatrick, J. B., Murdoch, G. H., Ball, M. J. and Roher, A. E. (1996) Water-soluble Aβ (N-40, N-42) oligomers in normal and Alzheimer disease brains. J. Biol. Chem. **271**, 4077–4081 CrossRef PubMed

12 Lue, L. F., Kuo, Y. M., Roher, A. E., Brachova, L., Shen, Y., Sue, L., Beach, T., Kurth, J. H., Rydel, R. E. and Rogers, J. (1999) Soluble amyloid β peptide concentration as a predictor of synaptic change in Alzheimer's disease. Am. J. Pathol. **155**, 853–862 CrossRef PubMed

13 Mc Donald, J. M., Savva, G. M., Brayne, C., Welzel, A. T., Forster, G., Shankar, G. M., Selkoe, D. J., Ince, P. G. and Walsh, D. M. (2010) The presence of sodium dodecyl sulphate-stable Aβ dimers is strongly associated with Alzheimer-type dementia. Brain **133**, 1328–1341 CrossRef PubMed

14 McLean, C. A., Cherny, R. A., Fraser, F. W., Fuller, S. J., Smith, M. J., Beyreuther, K., Bush, A. I. and Masters, C. L. (1999) Soluble pool of Aβ amyloid as a determinant of severity of neurodegeneration in Alzheimer's disease. Ann. Neurol. **46**, 860–866 CrossRef PubMed

15 Freir, D. B., Nicoll, A. J., Klyubin, I., Panico, S., Mc Donald, J. M., Risse, E., Asante, E. A., Farrow, M. A., Sessions, R. B., Saibil, H. R. et al. (2011) Interaction between prion protein and toxic amyloid β assemblies can be therapeutically targeted at multiple sites. Nat. Commun. **2**, 1341–51 CrossRef

16 Jin, M., Shepardson, N., Yang, T., Chen, G., Walsh, D. M. and Selkoe, D. J. (2011) Soluble amyloid β-protein dimers isolated from Alzheimer cortex directly induce Tau hyperphosphorylation and neuritic degeneration. Proc. Natl. Acad. Sci. U.S.A. **108**, 5819–5824 CrossRef PubMed

17 O'Nuallain, B., Freir, D. B., Nicoll, A. J., Risse, E., Ferguson, N., Herron, C. E., Collinge, J. and Walsh, D. M. (2010) Amyloid β-protein dimers rapidly form stable synaptotoxic protofibrils. J. Neurosci. **30**, 14411–14419 CrossRef PubMed

18 Yamaguchi, T., Yagi, H., Goto, Y., Matsuzaki, K. and Hoshino, M. (2010) A disulfide-linked amyloid-β peptide dimer forms a protofibril-like oligomer through a distinct pathway from amyloid fibril formation. Biochemistry **49**, 7100–7107 CrossRef PubMed

19 Kok, W. M., Scanlon, D. B., Karas, J. A., Miles, L. A., Tew, D. J., Parker, M. W., Barnham, K. J. and Hutton, C. A. (2009) Solid-phase synthesis of homodimeric peptides: preparation of covalently-linked dimers of amyloid β peptide. Chem. Comm. **41**, 6228–6230 CrossRef

20 Balasubramanian, D. and Kanwar, R. (2002) Molecular pathology of dityrosine cross-links in proteins: structural and functional analysis of four proteins. Mol. Cell. Biochem. **234–235**, 27–38 CrossRef

21 Hensley, K., Maidt, M. L., Yu, Z., Sang, H., Markesbery, W. R. and Floyd, R. A. (1998) Electrochemical analysis of protein nitrotyrosine and dityrosine in the Alzheimer brain indicates region-specific accumulation. J. Neurosci. **18**, 8126–8132 PubMed

22 Al-Hilaly, Y. K., Williams, T. L., Stewart-Parker, M., Ford, L., Skaria, E., Cole, M., Bucher, W. G., Morris, K. L., Sada, A. A., Thorpe, J. R. and Serpell, L. C. (2013) A central role for dityrosine crosslinking of amyloid-β in Alzheimer's disease. Acta. Neuropathol. Comm. **1**, 83 CrossRef

23 Ali, F. E., Leung, A., Cherny, R. A., Mavros, C., Barnham, K. J., Separovic, F. and Barrow, C. J. (2006) Dimerisation of *N*-acetyl-L-tyrosine ethyl ester and Aβ peptides via formation of dityrosine. Free Radic. Res. **40**, 1–9 CrossRef PubMed

24 Galeazzi, L., Ronchi, P., Franceschi, C. and Giunta, S. (1999) *In vitro* peroxidase oxidation induces stable dimers of β-amyloid (1–42) through dityrosine bridge formation. Amyloid **6**, 7–13 CrossRef PubMed

25 Yoburn, J. C., Tian, W., Brower, J. O., Nowick, J. S., Glabe, C. G. and Van Vranken, D. L. (2003) Dityrosine cross-linked Aβ peptides: fibrillar β-structure in $A\beta^{1-40}$ is conducive to formation of dityrosine cross-links but a dityrosine cross-link in $A\beta^{8-14}$ does not induce β-structure. Chem. Res. Toxicol. **16**, 531–535 CrossRef PubMed

26 Finder, V. H., Vodopivec, I., Nitsch, R. M. and Glockshuber, R. (2010) The recombinant amyloid-β peptide $A\beta_{1-42}$ aggregates faster and is more neurotoxic than synthetic $A\beta_{1-42}$. J. Mol. Biol. **396**, 9–18 CrossRef PubMed

27 Walsh, D. M., Thulin, E., Minogue, A. M., Gustavsson, N., Pang, E., Teplow, D. B. and Linse, S. (2009) A facile method for expression and purification of the Alzheimer's disease-associated amyloid β-peptide. FEBS. J. **276**, 1266–1281 CrossRef PubMed

28 Moir, R. D., Tseitlin, K. A., Soscia, S., Hyman, B. T., Irizarry, M. C. and Tanzi, R. E. (2005) Autoantibodies to redox-modified oligomeric Aβ are attenuated in the plasma of Alzheimer's disease patients. J. Biol. Chem. **280**, 17458–17463 CrossRef PubMed

29 Betts, V., Leissring, M. A., Dolios, G., Wang, R., Selkoe, D. J. and Walsh, D. M. (2008) Aggregation and catabolism of disease-associated intra-Aβ mutations: reduced proteolysis of AβA21G by neprilysin. Neurobiol. Dis. **31**, 442–450 CrossRef PubMed

30 Hu, N. W., Smith, I. M., Walsh, D. M. and Rowan, M. J. (2008) Soluble amyloid-β peptides potently disrupt hippocampal synaptic plasticity in the absence of cerebrovascular dysfunction *in vivo*. Brain **131**, 2414–2424 CrossRef PubMed

31 Walsh, D. M., Lomakin, A., Benedek, G. B., Condron, M. M. and Teplow, D. B. (1997) Amyloid β-protein fibrillogenesis. Detection of a protofibrillar intermediate. J. Biol. Chem. **272**, 22364–22372 CrossRef PubMed

32 Lomakin, A. and Teplow, D. B. (2012) Quasielastic light scattering study of amyloid β-protein fibrillogenesis. Meth. Mol. Biol. **849**, 69–83 CrossRef

33 Studier, F. W. (2005) Protein production by auto-induction in high density shaking cultures. Protein Expr. Purif. **41**, 207–234 CrossRef PubMed

34 Delaglio, F., Grzesiek, S., Vuister, G. W., Zhu, G., Pfeifer, J. and Bax, A. (1995) NMRPipe: a multidimensional spectral processing system based on UNIX pipes. J. Biomol. NMR **6**, 277–293 CrossRef PubMed

35 Tamiola, K. and Mulder, F. A. (2011) ncIDP-assign: a SPARKY extension for the effective NMR assignment of intrinsically ordered proteins. Bioinformatics **27**, 1039–1040 CrossRef PubMed

36 Markley, J. L., Bax, A., Arata, Y., Hilbers, C. W., Kaptein, R., Sykes, B. D., Wright, P. E. and Wuthrich, K. (1998) Recommendations for the presentation of NMR structures of proteins and nucleic acids. IUPAC-IUBMB-IUPAB inter-union task group on the standardization of data bases of protein and nucleic acid structures determined by NMR spectroscopy. J. Biomol. NMR **12**, 1–23 CrossRef PubMed

37 Tamiola, K., Acar, B. and Mulder, F. A. A. (2010) Sequence-specific random coil chemical shifts of intrinsically disordered proteins. J. Am. Chem. Soc. **132**, 18000–18003 CrossRef PubMed

38 Tamiola, K. and Mulder, F. A. A. (2012) Using NMR chemical shifts to calculate the propensity for structural order and disorder in proteins. Biochem. Soc. Trans. **40**, 1014–1020 CrossRef PubMed

39 Kok, W. M., Cottam, J. M., Ciccotosto, G. D., Miles, L. A., Karas, J. A., Scanlon, D. B., Roberts, B. R., Parker, M. W., Cappai, R., Barnham, K. J. and Hutton, C. A. (2013) Synthetic dityrosine-linked β-amyloid dimers form stable, soluble, neurotoxic oligomers. Chem. Sci. **4**, 4449–4454 CrossRef

40 Bateman, R. J., Xiong, C., Benzinger, T. L., Fagan, A. M., Goate, A., Fox, N. C., Marcus, D. S., Cairns, N. J., Xie, X., Blazey, T. M. et al. (2012) Clinical and biomarker changes in dominantly inherited Alzheimer's disease. N. Eng. J. Med. **367**, 795–804 CrossRef

41 Buchhave, P., Minthon, L., Zetterberg, H., Wallin, A. K., Blennow, K. and Hansson, O. (2012) Cerebrospinal fluid levels of β-amyloid 1–42, but not of tau, are fully changed already 5 to 10 years before the onset of Alzheimer dementia. Arch. Gen. Psych. **69**, 98–106 CrossRef

42 Walsh, D. M. and Selkoe, D. J. (2004) Deciphering the molecular basis of memory failure in Alzheimer's disease. Neuron **44**, 181–193 CrossRef PubMed

43 Palop, J. J. and Mucke, L. (2010) Amyloid-β-induced neuronal dysfunction in Alzheimer's disease: from synapses toward neural networks. Nat. Neurosci. **13**, 812–818 CrossRef PubMed

44 Malencik, D. A., Sprouse, J. F., Swanson, C. A. and Anderson, S. R. (1996) Dityrosine: preparation, isolation, and analysis. Anal. Biochem. **242**, 202–213 CrossRef PubMed

45 Manavalan, P. and Johnson, Jr, W. C. (1987) Variable selection method improves the prediction of protein secondary structure from circular dichroism spectra. Anal. Biochem. **167**, 76–85 CrossRef PubMed

46 Wishart, D. S., Sykes, B. D. and Richards, F. M. (1992) The chemical shift index: a fast and simple method for the assignment of protein secondary structure through NMR spectroscopy. Biochemistry **31**, 1647–1651 CrossRef PubMed

47 Hoyer, W., Gronwall, C., Jonsson, A., Stahl, S. and Hard, T. (2008) Stabilization of a β-hairpin in monomeric Alzheimer's amyloid-β peptide inhibits amyloid formation. Proc. Natl. Acad. Sci. U.S.A. **105**, 5099–5104 CrossRef PubMed

48 Tycko, R. (2004) Progress towards a molecular-level structural understanding of amyloid fibrils. Curr. Opin. Struct. Biol. **14**, 96–103 CrossRef PubMed

49 Roher, A. E., Chaney, M. O., Kuo, Y. M., Webster, S. D., Stine, W. B., Haverkamp, L. J., Woods, A. S., Cotter, R. J., Tuohy, J. M., Krafft, G. A. et al. (1996) Morphology and toxicity of $A\beta_{1-42}$ dimer derived from neuritic and vascular amyloid deposits of Alzheimer's disease. J. Biol. Chem. **271**, 20631–20635 CrossRef PubMed

50 Smith, D. P., Ciccotosto, G. D., Tew, D. J., Fodero-Tavoletti, M. T., Johanssen, T., Masters, C. L., Barnham, K. J. and Cappai, R. (2007) Concentration dependent Cu^{2+} induced aggregation and dityrosine formation of the Alzheimer's disease amyloid-β peptide. Biochemistry **46**, 2881–2891 CrossRef PubMed

51 Vigo-Pelfrey, C., Lee, D., Keim, P., Lieberburg, I. and Schenk, D. B. (1993) Characterization of β-amyloid peptide from human cerebrospinal fluid. J. Neurochem. **61**, 1965–1968 CrossRef PubMed

52 Villemagne, V. L., Perez, K. A., Pike, K. E., Kok, W. M., Rowe, C. C., White, A. R., Bourgeat, P., Salvado, O., Bedo, J., Hutton, C. A. et al. (2010) Blood-borne amyloid-β dimer correlates with clinical markers of Alzheimer's disease. J. Neurosci. **30**, 6315–6322 CrossRef PubMed

53 Cohen, S. I., Linse, S., Luheshi, L. M., Hellstrand, E., White, D. A., Rajah, L., Otzen, D. E., Vendruscolo, M., Dobson, C. M. and Knowles, T. P. (2013) Proliferation of amyloid-β42 aggregates occurs through a secondary nucleation mechanism. Proc. Natl. Acad. Sci. U.S.A. **110**, 9758–9763 CrossRef PubMed

54 Jeong, J. S., Ansaloni, A., Mezzenga, R., Lashuel, H. A. and Dietler, G. (2013) Novel mechanistic insight into the molecular basis of amyloid polymorphism and secondary nucleation during amyloid formation. J. Mol. Biol. **425**, 1765–1781 CrossRef PubMed

55 Knowles, T. P., Waudby, C. A., Devlin, G. L., Cohen, S. I., Aguzzi, A., Vendruscolo, M., Terentjev, E. M., Welland, M. E. and Dobson, C. M. (2009) An analytical solution to the kinetics of breakable filament assembly. Science **326**, 1533–1537 CrossRef PubMed

56 Petkova, A. T., Ishii, Y., Balbach, J. J., Antzutkin, O. N., Leapman, R. D., Delaglio, F. and Tycko, R. (2002) A structural model for Alzheimer's β-amyloid fibrils based on experimental constraints from solid state NMR. Proc. Natl. Acad. Sci. U.S.A. **99**, 16742–16747 CrossRef PubMed

57 Petkova, A. T., Leapman, R. D., Guo, Z., Yau, W. M., Mattson, M. P. and Tycko, R. (2005) Self-propagating, molecular-level polymorphism in Alzheimer's β-amyloid fibrils. Science **307**, 262–265 CrossRef PubMed

58 Petkova, A. T., Yau, W. M. and Tycko, R. (2006) Experimental constraints on quaternary structure in Alzheimer's β-amyloid fibrils. Biochemistry **45**, 498–512 CrossRef PubMed

59 Yu, L., Edalji, R., Harlan, J. E., Holzman, T. F., Lopez, A. P., Labkovsky, B., Hillen, H., Barghorn, S., Ebert, U., Richardson, P. L. et al. (2009) Structural characterization of a soluble amyloid β-peptide oligomer. Biochemistry **48**, 1870–1877 CrossRef PubMed

60 Sandberg, A., Luheshi, L. M., Sollvander, S., Pereira de Barros, T., Macao, B., Knowles, T. P., Biverstal, H., Lendel, C., Ekholm-Petterson, F., Dubnovitsky, A. et al. (2010) Stabilization of neurotoxic Alzheimer amyloid-β oligomers by protein engineering. Proc. Natl. Acad. Sci. U.S.A. **107**, 15595–15600 CrossRef PubMed

61 Vandersteen, A., Masman, M. F., De Baets, G., Jonckheere, W., van der Werf, K., Marrink, S. J., Rozenski, J., Benilova, I., De Strooper, B., Subramaniam, V. et al. (2012) Molecular plasticity regulates oligomerization and cytotoxicity of the multipeptide-length amyloid-β peptide pool. J. Biol. Chem. **287**, 36732–36743 CrossRef PubMed

62 Kuperstein, I., Broersen, K., Benilova, I., Rozenski, J., Jonckheere, W., Debulpaep, M., Vandersteen, A., Segers-Nolten, I., Van Der Werf, K., Subramaniam, V. et al. (2010) Neurotoxicity of Alzheimer's disease Aβ peptides is induced by small changes in the Aβ42 to Aβ40 ratio. EMBO J. **29**, 3408–3420 CrossRef PubMed

63 Pauwels, K., Williams, T. L., Morris, K. L., Jonckheere, W., Vandersteen, A., Kelly, G., Schymkowitz, J., Rousseau, F., Pastore, A., Serpell, L. C. and Broersen, K. (2012) Structural basis for increased toxicity of pathological Aβ42:Aβ40 ratios in Alzheimer disease. J. Biol. Chem. **287**, 5650–5660 CrossRef PubMed

64 De Strooper, B. (2010) Proteases and proteolysis in Alzheimer disease: a multifactorial view on the disease process. Physiol. Rev. **90**, 465–494 CrossRef PubMed

65 Roberts, B. R., Ryan, T. M., Bush, A. I., Masters, C. L. and Duce, J. A. (2012) The role of metallobiology and amyloid-β peptides in Alzheimer's disease. J. Neurochem. **120**, 149–166 CrossRef PubMed

Received 18 February 2014/14 April 2014; accepted 1 May 2014
Published as BJ Immediate Publication 1 May 2014, doi:10.1042/BJ20140219

Biochem. J. (2014) **461**, 413–426 (Printed in Great Britain) doi:10.1042/BJ20140219

online data

SUPPLEMENTARY ONLINE DATA

Aβ dimers differ from monomers in structural propensity, aggregation paths and population of synaptotoxic assemblies

Tiernan T. O'MALLEY*†, Nur Alia OKTAVIANI‡, Dainan ZHANG§, Aleksey LOMAKIN‖, Brian O'NUALLAIN*, Sara LINSE¶, George B. BENEDEK‖, Michael J. ROWAN§, Frans A. A. MULDER‡**[1] and Dominic M. WALSH*[1]

*Laboratory for Neurodegenerative Research, Center for Neurologic Diseases, Brigham and Women's Hospital, and Harvard Medical School, Boston, MA 02115, U.S.A.
†School of Biomolecular and Biomedical Science, University College Dublin, Dublin 4, Republic of Ireland
‡Groningen Biomolecular Sciences and Biotechnology Institute, University of Groningen, 9749 AB Groningen, The Netherlands
§Department of Pharmacology and Therapeutics, Trinity College, Dublin 2, Ireland
‖Department of Physics and Materials Processing Center, Massachusetts Institute of Technology, Cambridge, MA 02139, U.S.A.
¶Department of Biophysical Chemistry, Lund University, SE221 00 Lund, Sweden
**Interdisciplinary Nanoscience Center (iNANO), Department of Chemistry, Aarhus University, DK-8000 Aarhus C, Denmark

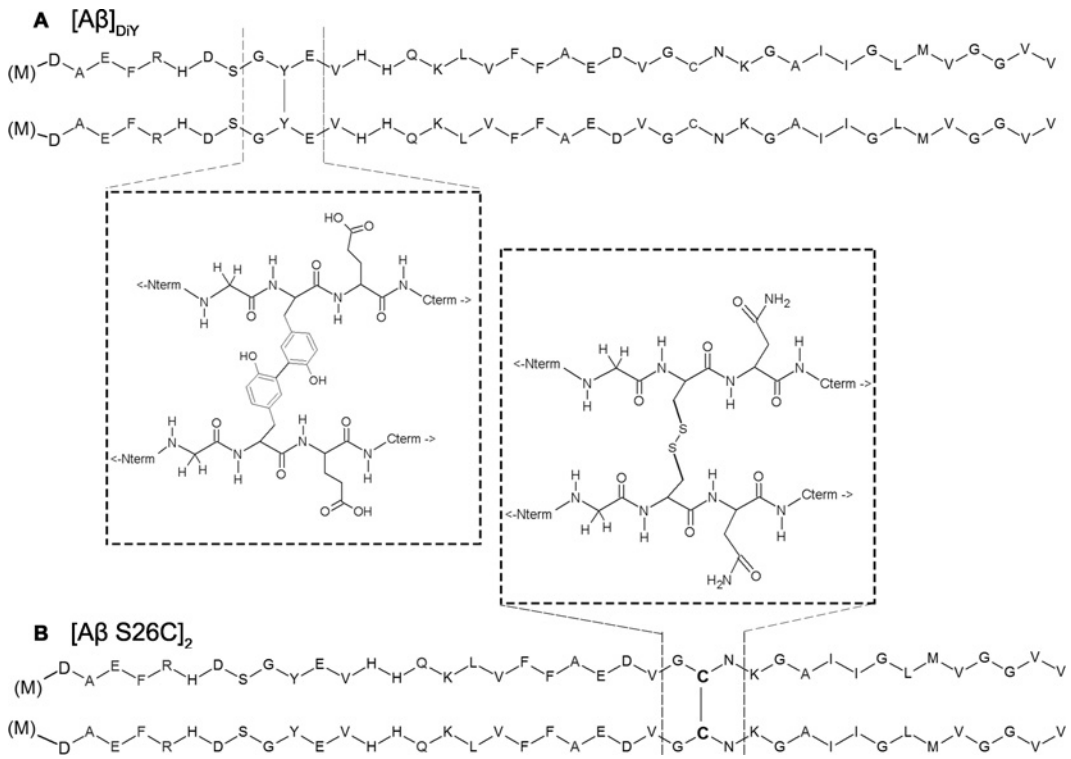

Figure S1 Schematic representation of [Aβ]$_{DiY}$ and [AβS26C]$_2$

The sequence of 1–40 long dimers are shown, with the position of the exogenous methionine residue present in recombinant peptides indicated by (M). The chemical structure of the cross-links are provided in the broken-lined boxes.

[1] Correspondence may be addressed to either of these authors (email fmulder@chem.au.dk or dwalsh3@partners.org).

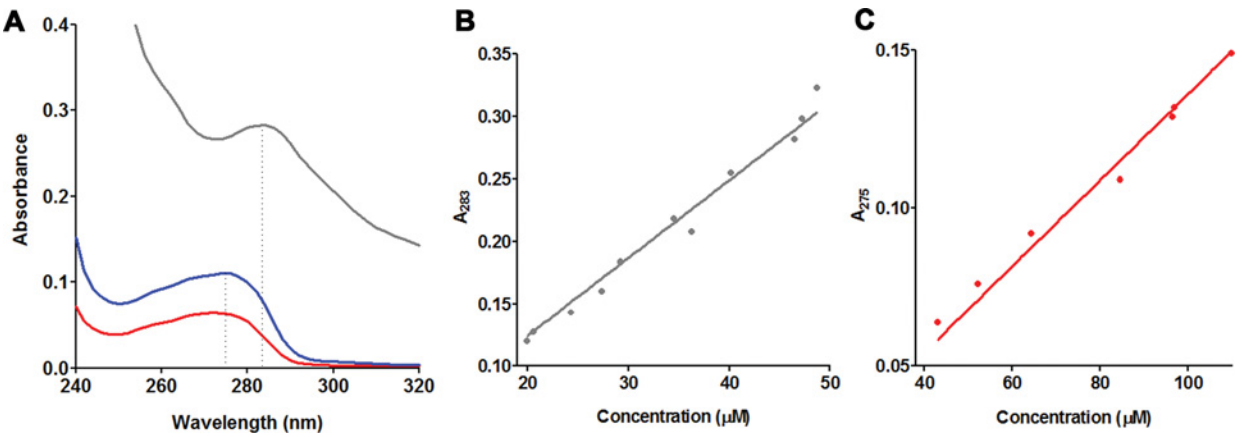

Figure S2 Determination of the molar extinction coefficients for Aβ(1–40) and [Aβ(1–40)]$_{DiY}$

Aβ(1–40) (red), [Aβ(1–40)]$_{DiY}$ (grey) and [Aβ(1–40)S26C]$_2$ (blue) were SEC-isolated in 20 mM sodium phosphate, pH 8.0, and diluted to 45 μM using the same buffer. (**A**) Absorbance spectra were obtained and the absorbance maxima (λ_{max}) were determined. (**B**) A peak fraction sample of SEC-isolated [Aβ(1–40)]$_{DiY}$ was diluted 90–40 % with 20 mM sodium phosphate, pH 8.0. For each sample, the absorption at 283 nm was recorded. Quantitative amino acid analysis determined concentration (the average of duplicate experiments) was plotted compared with A_{283} and the molar absorption coefficient (ε_{283}) calculated from the slope of the line. (**C**) An identical experiment was conducted using Aβ(1–40) and the ε_{275} for Aβ monomer determined. The R^2 values for both plots are >0.99. ε_{283} for [Aβ(1–40)]$_{DiY}$ is 6244 $M^{-1}\cdot cm^{-1}$ and ε_{275} for Aβ(1–40) is 1361 $M^{-1}\cdot cm^{-1}$. Because the absorbance spectrum for [Aβ(1–40)S26C]$_2$ is identical to that of Aβ(1–40), the ε_{275} for [Aβ(1–40)S26C]$_2$ was not experimentally determined.

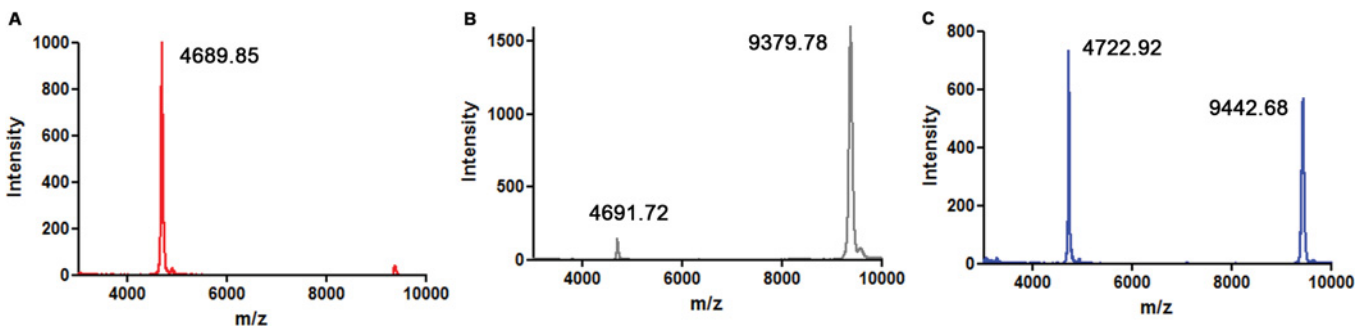

Figure S3 MS reveals efficient incorporation of ^{13}C and ^{15}N into Aβ(M1–40), [Aβ(M1–40)]$_{DiY}$ and [Aβ(M1–40)S26C]$_2$

MALDI–TOF analysis of isotopically labelled peptide indicates that (**A**) [^{13}C,^{15}N]Aβ(M1–40) had a product mass of 4688.85, 99.5 % of the theoretical mass of fully labelled [^{13}C,^{15}N]Aβ(M1–40). Similarly, (**B**) [Aβ(M1–40)]$_{DiY}$ and (**C**) [Aβ(M1–40)S26C]$_2$ yield masses of 9379.78 (99.5 %) and 9442.68 (99.9 %) respectively.

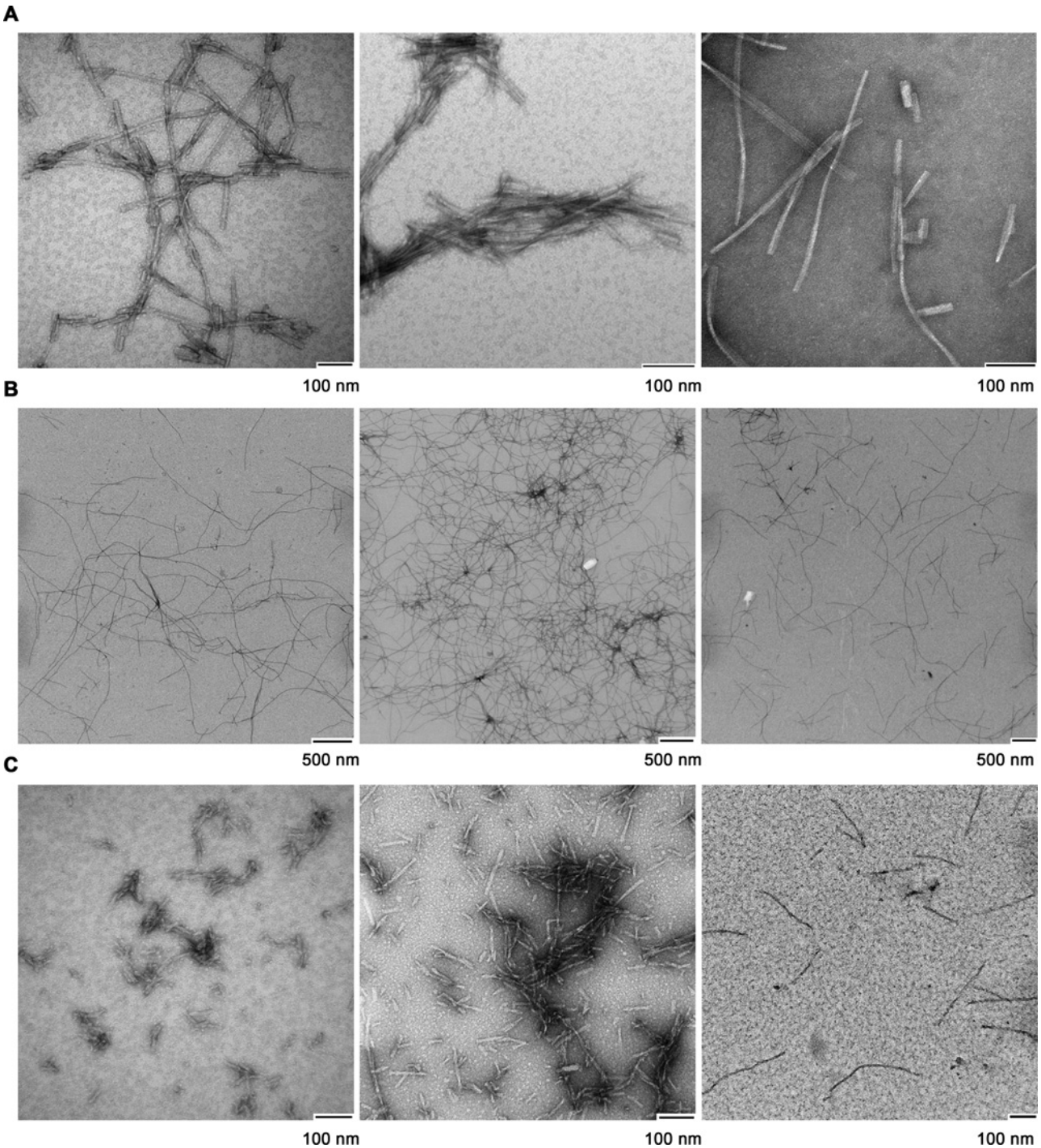

Figure S4 Electron micrographs of end point samples of Aβ(1–40), $[Aβ(1–40)]_{DiY}$ and $[Aβ(1–40)S26C]_2$

End point samples incubated in the absence of ThT were used for negative contrast EM. Images shown for (**A**) Aβ(1–40), (**B**) $[Aβ(1–40)]_{DiY}$ and (**C**) $[Aβ(1–40)S26C]_2$, three fields from two separate sample preparations are shown for each peptide. Note that $[Aβ(1–40)]_{DiY}$ samples are shown at lower magnification because this peptide consistently formed very long fibrils.

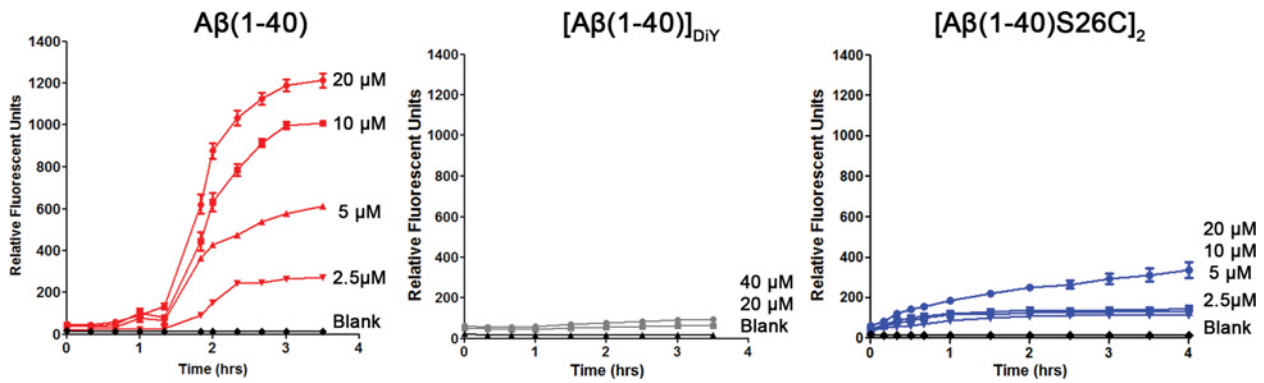

Figure S5 Aβ(1–40), [Aβ(1–40)]$_{DiY}$ and [Aβ(1–40)S26C]$_2$ exhibit different extents of ThT binding in the first 3 h of incubation

Exponded view of the data presented in Figure 1 in the main text. Following 3 h of incubation at 37°C with shaking, Aβ(1–40) reached its maximal fluorescence. In contrast, [Aβ(1–40)]$_{DiY}$ exhibits no ThT change over this time frame, whereas [Aβ(1–40)S26C]$_2$ steadily increases with no apparent lag phase. Values are the mean±S.E.M.

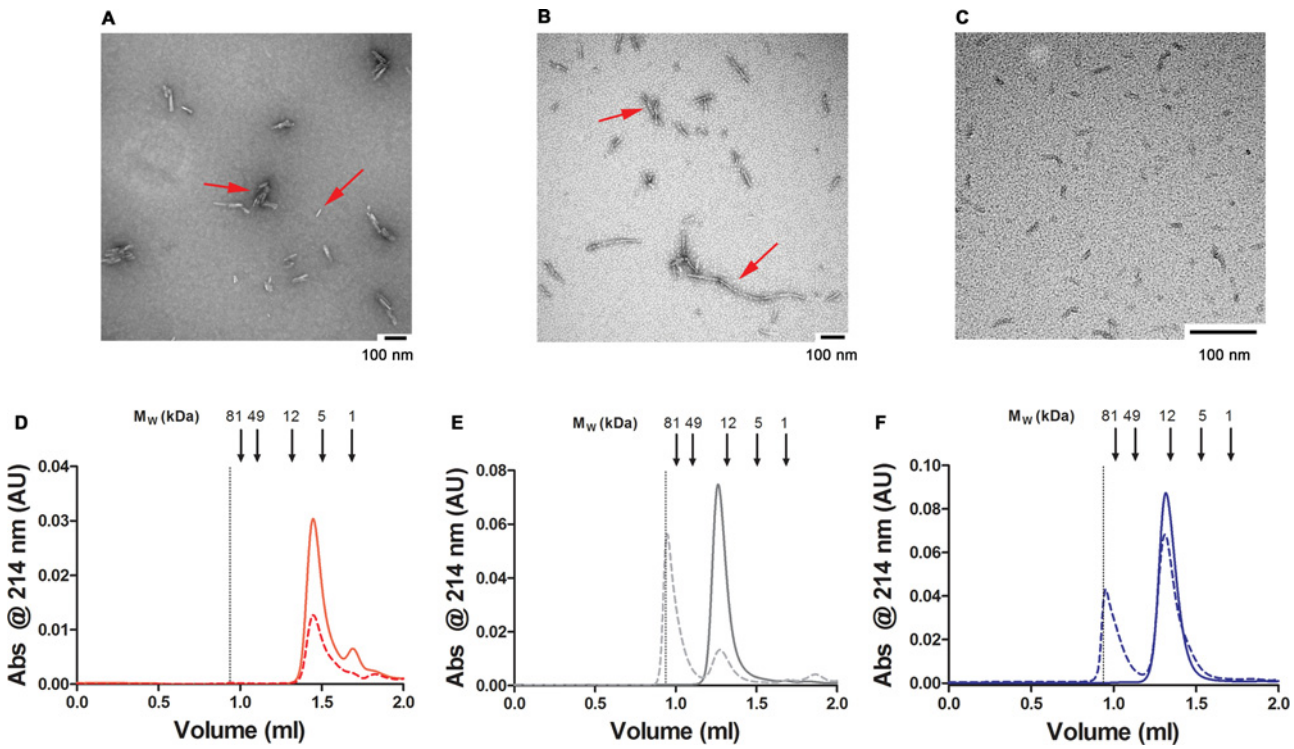

Figure S6 EM and analytical-SEC characterization of Aβ(1–40) and [Aβ(1–40)]$_{DiY}$ used for LTP experiments

Aggregated (**A**) Aβ(1–40), (**B**) [Aβ(1–40)]$_{DiY}$ and (**C**) [Aβ(1–40)S26C]$_2$ were visualized by negative contrast EM. Red arrows are used to point out aggregates with different morphologies. Samples were centrifuged at 16000 ***g*** for 30 min and used for analytical SEC at $t = 0$ (continuous line) and $t_{1/2\,max}$ (dashed line) and eluted in 20 mM sodium phosphate, pH 8.0. (**D**) Aβ(1–40), (**E**) [Aβ(1–40)]$_{DiY}$ and (**F**) [Aβ(1–40)S26C]$_2$. The void volume (0.95 ml) is indicated with a dotted vertical line and the elution of LDS (linear dextran standards) is indicated by arrows. AU, absorbance units.

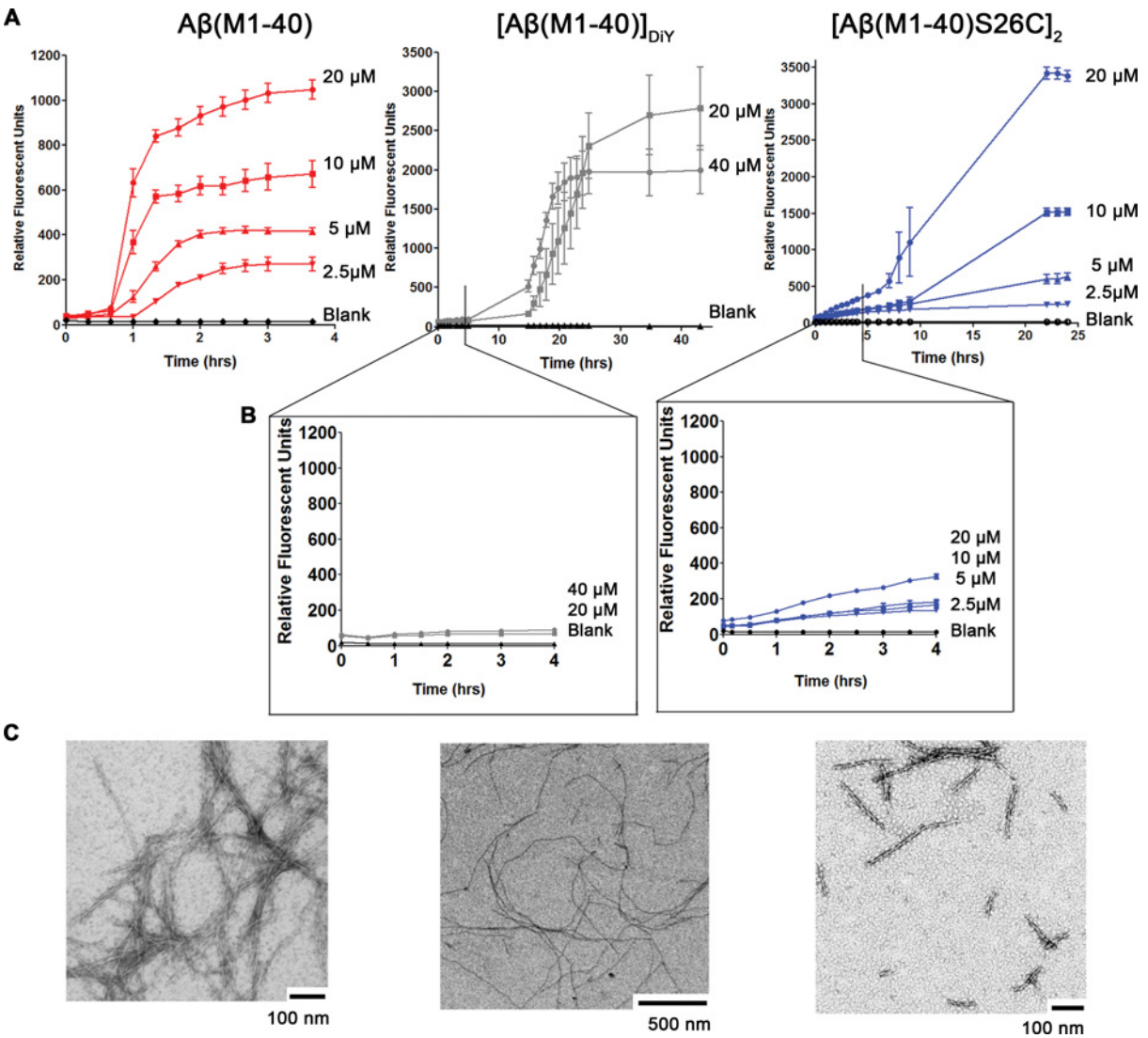

Figure S7 Recombinantly produced Aβ(M1–40), $[Aβ(M1–40)]_{DiY}$ and $[Aβ(M1–40)S26C]_2$ aggregate in a manner highly similar to chemically synthesized peptide

(**A**) SEC-isolated recombinant peptides were analysed by monitoring ThT fluorescence following incubation at 37°C with shaking as done exactly for chemically synthesized peptides. (**B**) Expanded view (0–4 h) for $[Aβ(M1–40)]_{DiY}$ (grey) and $[Aβ(M1–40)S26C]_2$ (blue) plotted on the same scale as Aβ(M1–40). (**C**) Samples of the end-point interval for Aβ(M1–40) (left-hand panel), $[Aβ(M1–40)]_{DiY}$ (middle panel) and $[Aβ(M1–40)S26C]_2$ (right-hand panel) were visualized by negative contrast EM. The aggregation time course and products are highly similar to those produced when chemically synthesized peptides are used. Values are the mean±S.E.M.

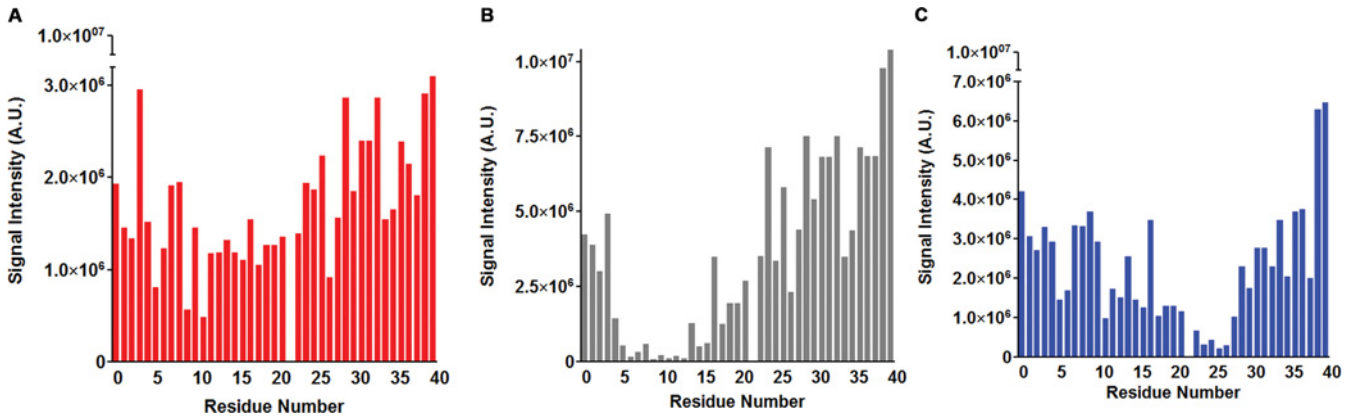

Figure S8 Covalent dimer formation restricts chain mobility around the attachment point

$^{13}C\alpha$,$^{1}H\alpha$ cross-peak signal intensities derived from (^{13}C,^{1}H)-HSQC spectra for (**A**) Aβ(M1–40), (**B**) [Aβ(M1–40)]$_{DiY}$ and (**C**) [Aβ(M1–40)S26C]$_2$ at pH 8.0. For [Aβ(M1–40)]$_{DiY}$, mobility restriction is found to occur at residue number 10 and over a range of residues 5–12, whereas restricted mobility for [Aβ(M1–40)S26C]$_2$ is observed for the position close to residue 26, and over a range of residues 23–27. Owing to overlapping peaks, a few signal intensities are not reported. AU, absorbance units.

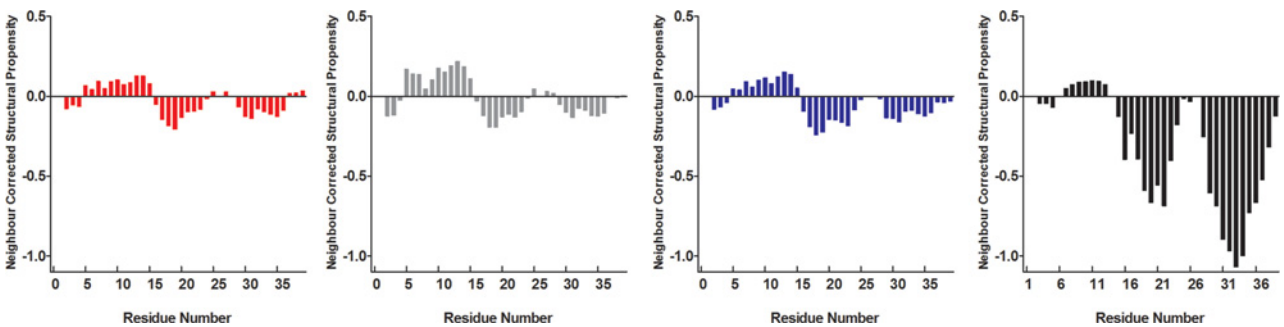

Figure S9 Aβ monomer and covalently cross-linked dimers structural propensity compared with the Aβ(1–40)–ZAβ_3 β-sheet complex

Structural propensity of Aβ(M1–40) (red), [Aβ(M1–40)]$_{DiY}$ (grey) and [Aβ(M1–40)S26C]$_2$ (blue) at pH 8.0 as calculated using ncSPC compared with the Aβ(1–40)–ZAβ3 complex (black) reported by Hoyer et al. [1] (chemical shift data taken from the Biological Magnetic Resonance Bank ID 17159). Positive values indicate helical propensity and negative values predict β-sheet conformation.

REFERENCE

1 Hoyer, W., Gronwall, C., Jonsson, A., Stahl, S. and Hard, T. (2008) Stabilization of a β-hairpin in monomeric Alzheimer's amyloid-β peptide inhibits amyloid formation. Proc. Natl. Acad. Sci. U.S.A. **105**, 5099–5104 CrossRef PubMed

Received 18 February 2014/14 April 2014; accepted 1 May 2014
Published as BJ Immediate Publication 1 May 2014, doi:10.1042/BJ20140219